AFRICA CENTER OF EXCELLENCE FOR WATER MANAGEMENT
ADDIS ABABA UNIVERSITY

IMPACTS OF LAND USE LAND COVER AND CLIMATE CHANGE ON SURFACE WATER BALANCECOMPONENTS OF GOBELE WATERSHED IN WABE SHEBELLE BASIN, ETHIOPIA.

MSC. THESIS

By

Iradukunda Valentine

A Master's thesis submitted to the Africa Center of Excellence for Water Management, Addis Ababa University in partial fulfillment of the requirements for The Degree of Master of Science in Water Management (Hydrology and Water Resources).

July, 2024

Addis Ababa, Ethiopia

Africa Center of Excellence for Water Management

Addis Ababa University

School of Graduate Studies

IMPACTS OF LAND USE LAND COVER AND CLIMATE CHANGE ON SURFACE WATER BALANCECOMPONENTS OF GOBELE WATERSHED IN WABE SHEBELLE BASIN, ETHIOPIA.

By:

Iradukunda Valentine

A Master's thesis submitted to the Africa Center of Excellence for Water Management, Addis Ababa University in partial fulfillment of the requirements for The Degree of Master of Science in Water Management (Hydrology and Water Resources)

DECLARATION

I, **Iradukunda Valentine** with registration number GSR/3072/15, hereby declare that this Msc research proposal titled" **Impacts of Land Use Land Cover and Climate Change on Surface Water Balance Components of Gobele watershed in Wabe Shebelle Basin, Ethiopia**" has been created by me and is not being submitted to any other university for the purpose of receiving a degree. The thesis's content is original, and any instances in which it draws from the work of other academics have been duly acknowledged.

Student's name	**Signature**	**Date**
Iradukunda Valentine	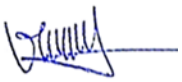	12/07/2024

AFRICA CENTER OF EXCELLENCE FOR WATER MANAGEMENT
ADDIS ABABA UNIVERSITY

IMPACTS OF LAND USE LAND COVER AND CLIMATE CHANGE ON SURFACE WATER BALANCE COMPONENTS OF GOBELE WATERSHED IN WABE SHEBELLE BASIN, ETHIOPIA.

By:

Iradukunda Valentine

A MASTER'S THESIS SUBMITTED
TO
AFRICA CENTER OF EXCELLENCE FOR WATER MANAGEMENT

ADDIS ABABA UNIVERSITY

APPROVED BY BOARD OF EXAMINERS

This is to certify that we have read this MSc research and that in our opinion; it is fully adequate, in scope and quality, as a Master's thesis for The Degree of Master of Science in Water Management (Hydrology and Water Resources).

Advisor

Name **Dr. Habtamu Hailu** Signature  ___Date____14th July 2024

External Examiner

Name **Dr.Getachew Tegegne** Signature  Date__ 21st July 2024

Internal Examiner

Name **Dr.Dessie Nedaw** Signature___  __ Date___17th July 2024_____

Chairperson
Name **Dr.Getachew Dagnew**__ Signature_____ Date_____

ACKNOWLEDGEMENT

Firstly, I give thanks and glory to the Almighty God for giving me good health and showering me with blessings during my study period that helped me to fully accomplish my study.

I want also to express my gratitude to my supervisor Dr. Habtamu Hailu for guiding me and valuable advice throughout the whole research work. His motivation and availability to review the work with valuable advice at each step were very helpful in accomplishing the work on time.

I would like to thank the World Bank through the Africa Center of Excellence for Water Management for sponsoring my studies as well as thesis work. I have learned a lot in the program which will help me in my future career to be a valuable person in society.

Furthermore, I raise my heartfelt gratitude to my parents and siblings for showing me unconditional love and distant support in everything through their prayers and words of encouragement that have guided me.

Last but not least, I extend my appreciation to my colleagues, friends and family for showing love and care during my study period.

TABLE OF CONTENTS

LIST OF TABLES

LIST OF FIGURES

LIST OF APPENDICES

LIST OF ABBREVIATIONS

LULC	Land Use Land Cover
USGS	United States Geological Survey
TM	Thematic Mapper
OLI	Operational Land Imagery
ETM	Enhanced Thematic Mapper
STRM	Shuttle Radar Topography Mission
SWAT	Soil and Water Assessment Tool
SWAT-CUP	Calibration and Uncertainty Program
SUFI-2	Sequential Uncertainty Fitting Ver.2
ERDAS	Earth Resources Data Analysis System
GIS	Geographical Information System
CA	Cellular Automata
ARS	Agricultural Research Service
RS	Remote Sensing
SSPs	Shared socioeconomic pathways
GCM	General/ Global Circulation Models
RCPs	Representative Concentration Pathways
LCM	Land Change Modeler
DEM	Digital Elevation Model
MK	Mann-Kendall test
HRU	Hydrological Response Units
FAO	Food and Agriculture Organization
MoWIE	Ministry of Water, Irrigation and Energy
NMAE	National Meteorological Agency of Ethiopia
Cmhyd	Climate model data for hydrologic modeling
CMIP5	Coupled model Inter-comparison project phase five
CMIP6	Coupled model Inter-comparison project phase six
GCM	General/ Global Circulation Models
NSE	Nash-Sutcliffe efficiency Coefficient
R^2	Coefficient of Determination
IPCC	Intergovernmental Panel on Climate Change
SRES	Special Report Emission Scenarios

ABSTRACT

Changes in land use land cover and climate are important global challenges due to the impact on water balance components. Climate change is caused by a change in greenhouse gas concentration due to natural and anthropogenic forcing. This study was conducted in Gobele watershed of the Wabe Shebelle River Basin, Ethiopia. It evaluated the individual and combined impacts of both climate change and LULC change on water balance components. Three historical periods (1990, 2005, and 2020) of Landsat satellite images of the study area were used for LULC analysis using ArcGIS. The Soil and Water Assessment Tool (SWAT) was utilized for the simulation of water balance parameters. Maximum likelihood classification was used to classify historical LULC, and the Cellular Automata-Markov Chain model in land change modeler was used to generate the future LULC forecast. The Statistical Downscaling Model (SDSM) was utilized to generate high-resolution future climatic data from well performed four climate models (ACCESS-CM2, MPI-ESM1-2-LR, ICHEC–EC–EARTH, and CanESM2) and their multi-model ensemble mean was used for impact assessment of climate and LULC change on water balance components. The hydrological response of the basin was evaluated using three scenarios: LULC change alone, climate change alone, and combined climate and LULC change. The future periods were divided into the midterm future (2040–2070) and the distant future (2071-2100). According to the CA-Markov chain model's projection of the LULC change, over the study period, agricultural land and settlement areas will increase while grassland/shrub land and forest land are expected to decline. The climate projection result indicates an increase in both Tmax and Tmin under SSP5.8.5 and SSP2-4.5 and SSP5-8.5 climate scenarios in the midterm (2040-2070) and distant future (2071-2100). Likewise, precipitation will show an increasing pattern in the basin. Under SSP5-8.5, evapotranspiration will increase more by climate change than by LULC change during the baseline period (1990-2020). Furthermore, both stream flow and water yield will increase under all scenarios. Moreover, the SWAT model performed satisfactorily in simulating discharge during the calibration and validation periods at the designated gauging station in the Gobele watershed with R^2 and NSE values of 0.86, 0.76, and 0.91, 0.69, respectively. Thus, the results of this study provide valuable information to planners and policymakers for sustainable planning of water resources in the Gobele watershed in the face of climate and LULC change.

Keywords: Climate change, LULC, Gobele watershed, SWAT, Water balance

1. INTRODUCTION

1.1. Background

The two most significant interconnected resources on Earth are land and water. Changes in land use, land cover and climatic variability have significant impacts on socioeconomic activityand the management of water resources. They are placing significant pressure on the quantity and quality of water resources and thus lead to extreme hydrological events that have an impact on the elements of the water balance (Belihu et al., 2020; Huyen et al., 2017). Water balance components indicate water as it flows through different global systems and storages by means of several forms and processes. They include precipitation, runoff, evapotranspiration, infiltrations, percolation, interflow, recharge, and discharge of groundwater (Access et al., 2008).

Land use/land cover (LULC) change can occur as a total transition from one land use type to another or as a minor adjustment, both of which have substantial effects on biodiversity, hydrology, soil erosion, and microclimate that can lead to the degrading of watersheds and can have significant impacts on water balance components that are dynamic in space and time (Kumaet al., 2023). Since the 18thcentury, human activity has significantly increased the amount of greenhouse gases (GHGs) in the atmosphere, contributing to climate change (Reshmidevi et al., 2018).

The Intergovernmental Panel on Climate Change (IPCC) (IPCC, 2021) study states that since the Fifth Assessment study (AR5), there has been an increase in the global surface temperature, mostly because of increased warming that occurred between 2003 and 2012 (+0.19 °C). Furthermore, general circulation models (GCMs) simulations of future climate for the middle to end of the twenty-first century indicate a global warming trend that impacts the water balance components (Uniyal et al., 2015).

Many studies have been conducted on the relationship between climate change and land use/cover change worldwide, such as Europe, the United States, Asia and Africa (Mitiku et al., 2023; Lee et al., 2011; Manakos & Braun, 2014; Tesfaw et al., 2023; Wainwright et al., 2021).

The expansion of agricultural land influenced by rapid population growth and temperature increases has been recognized as a primary driver of LULC and climate change.

According to several research works on climate and land use land cover change impacts on

water balance components in Ethiopia, many sides of the country have seen quick and dramatic land use and climate change since the last part of the 20th century (Belay & Mengistu, 2021; Getachew et al.,2021; Mitiku et al., 2023; Woldemariam & Harka, 2020; Yohannes et al., 2018).

About how changes in land use and cover affect the components of the water balance, an increase in mean annual flow has been reported from different corners of Ethiopia (Welde & Gebremariam, 2017). Increases in soil loss due to LULC Change have also been reported (Kyu et al., 2016; Welde & Gebremariam, 2017). Land degradation increases people's vulnerability to climate change by reducing agricultural productivity (Woodfine, 2009).

Furthermore, the potentially negative impacts of climate change could bring long-term effects in all aspectsof the hydrologic cycle, such as rainfall, runoff, evapotranspiration, peak flows, and flow routing time andrunoff volumes (Adams-Schoen et al., 2015). Ethiopia, like other developing countries, is more likely to be affected by future land use and climate change because of its economic reliance on rain-fed agriculture, population increases, and geographic conditions.

Due to that, the climate and land use/cover change impact assessment on water balance components is required, and it involves projections of climatic variables (temperature and rainfall) at on both a local and global levels (Ghosh & Mujumdar, 2009).

A recent Intergovernmental Panel on Climate Change (IPCC) indicated over 100% warming potential for equatorial East Africa. The temperatures will be 2°C warmer than the 1981-2000 average in the mid-to-late 21st century (Trisos et al., 2022). As indicated by the IPCC, developing countries will be more affected by climate change due to theireconomic, climatic and geographic settings (IPCC, 2014).

In the current study, the Gobele watershed, which is found in the Wabe Shebelle River basin in Ethiopia, supports the livelihoods of millionsof people who depend on its surface water resources (Guduru & Jilo, 2022). However, the watershed is undergoing rapid land use transformations due to various socioeconomic and environmental factors, such as population pressure, agricultural development, deforestation, and urbanization (Woldemariam et al., 2018). These transformations, in turn, lead to climatic changessuch as floods and droughts in the study area.

Evaluating the impact of land use and climate change on water balance components of a watershed is a challenge due to its complex relationship with landscape, morphology and

hydrology. Therefore, the land use planner and water resource manager, aswell as a decision maker in the field of study, need to have a good understanding of and quantify these impacts at the catchment scale. Several researchers have evaluated the individual impact of either climate or LULC change on water balance components in different watersheds in Ethiopia (Fita & Abate, 2022a; Orkodjo et al., 2022; Woldemariam & Harka, 2020; Yohannes et al., 2018).

It is vital to comprehend the collective effects of these variables on the constituents of the water balance, though. In order to assess the effects of land use and climate change on the components of the water balance in the Gobele watershed, Wabe Shebele River Basin, Ethiopia, this study was conducted.

1.2. Problem Statement

Watershed hydrology is the key factor for both effective and sustainable water resource planning, development and management. There are different factors governing watershed hydrology, like land use, land cover and climate changes. They are putting pressure on both water quantity and quality by affecting evapotranspiration, soil moisture content and river discharge (Mitiku et al., 2023).

Global warming caused by huge emissions of greenhouse gases has been observed over past decades,which is highly associated with changes in temperature and precipitation patterns. This, in turn, leads to the occurrence of unprecedented extreme hydrological events (flood and drought). Due to the variability of rainfall both in time and space, the sector is observed to be critically affected by this phenomenon. Consequently, water balance components such as evapotranspiration, water yield and stream flows are negatively impacted, and societal demand is increasing due to population growth.

This leads to the destruction of infrastructure in the area as well as causing water stress (Gurara et al., 2021). Moreover, the previous studies have not yet performed LULC and climate change detection and their impact on water balance components of the Gobele catchment. This suggests that a thorough study of the Gobele watershed is necessary to know the impacts caused by the future temperature and rainfall change as well as the land use land cover on water parameters for various time intervals.

In general, along with the land use land cover change, it is crucial to perform the trend and homogeneity test analysis of temperature and rainfall at precise spatial and temporal scales. The Representative Concentration Pathways (RCPs) 4.5 and 8.5 utilized in earlier research in nearby watersheds need to be revised to reflect the current climatic scenarios (SSP 2-4.5 and SSP 5-8.5). The studies also assumed that land use and land cover remained unchanged (Fita & Abate, 2022a; Gurara et al., 2021).

Currently, the Gobele watershed in the Wabe Shebelle River Basin, Ethiopia, is exposed to land use and climate change. This has impacts on the hydro-climatic variables, such as rainfall distribution, temperature variation, and evapotranspiration rate. Thus, by examining the effects of both individual and combined climate and LULC change on water balance components, this study aimed to close a research gap.

1.3 Research Objectives

1.3.1 General Objective

The main objective of the study was to assess the impact of climate and LULC change on water balance components in the Gobele watershed, Wabe-Shebelle River basin, Ethiopia.

1.3.2 Specific Objectives

- To analyze the land use land cover change of the Gobele watershed in the Wabi-Shebelle basin using RS and GIS.
- To evaluate the performance of the SWAT model in the study area for different periods.
- To evaluate separate and combined land use land cover and climate change impacts on water balance components in the Gobele watershed.

1.4 Research Questions

This research will be done to answer the following questions:

- What are the LULC change trends in the study area?
- What are the projected changes in precipitation and temperature in the study area in the midterm and far period?
- What is the performance of the SWAT model in water balance components under different LULC and climate change?

- What is the combined effect of LULC and climate change on the waterbalance components in the study area?

1.5 Significance of the Study

LULC and climate change are increasing due to population growth, expansion of agriculture, overgrazing and urbanization (Yohannes et al., 2018). Managing water resources sustainably and their conservation leads to better health for society, and it is a solution to the water stress problem. As a result, the purpose of this research was to provide useful information to planners, decision-makers, and anyone else who is interested in learning more about how land use and climate change will affect future components of the water balance. The results of this study are also useful to those who look forward to conducting related research in the future.

1.6 Scope and Limitations of the Study

This study focused on evaluating the effects of land use, land cover, and climate change on surface hydrology (stream flow, water yield, and evapotranspiration). It employed the SWAT model and climate data in up-to-date climate change scenarios in CMIP6 together with satellite images to assess the effects of change in land use and cover and climate on the water balance components in the Gobele watershed. Based on the nature of the CMIP6 climate models, it is advised to be used in near future prediction. Due to this, the current study was not able to evaluate the changes in temperature and rainfall for the very close future period from 2025 to 2039.

2. LITERATURE REVIEW

2.1 Concept of Water Balance Component

The term water balance component refers to changes in a water body's status and features that occur often throughout time and space and go through several phases, such as seasonal changes. Moreover, there is a change in the levels and speeds of river flow throughout time, as well as water levels in marshes, lakes, reservoirs, and rivers. Seasonal fluctuations in climate are closely correlated with the components of water balance. In areas with a warm climate, atmospheric precipitation and evaporation have the greatest impact on the hydrology; in areas with a cold or temperate climate, air temperature is a major determinant (Thanapakpawin et al., 2007).

Water balance components in watersheds are influenced by a complex interplay of factors such as land use land cover (LULC), climate, topography, and soil properties. Modifications to LULC, especially transformations from one form to another, can have profound implications for hydrological processes that are spatio-temporally dynamic. Several studies have shown that changes in LULC and climate can have significant impacts on catchment hydrology (Chaemiso et al., 2016). For example, changes in LULC and climate have been reported to possess a major influence on hydrological processes in various regions of Ethiopia (Fita & Abate, 2022a; Kim & Kaluarachchi, 2009; Tola & Shetty, 2021).

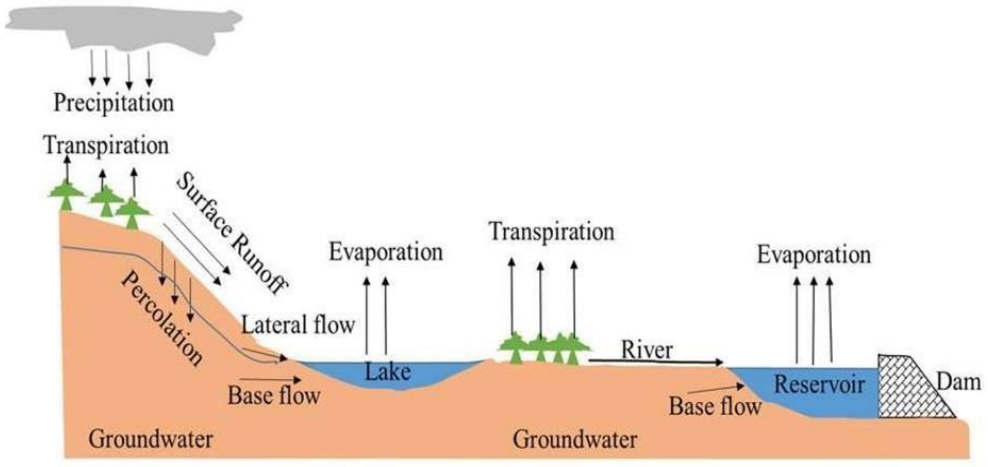

Figure 2.1 Water Balance Components

2.2 Concept of Land Use Land Cover

Land cover is the physical and biophysical properties or conditions of the Earth's surface and its immediate vicinity, as well as the distribution of vegetation, water, deserts, ice, and other physical features of land. This includes those created solely by human activity, such as settlements. Land use is the original use or managing land cover types by humans. Land Use/Land Cover (LULC) is one of the most important parts of the terrestrial environment system (Lin et al., 2009).

Land use and land-cover changes have a direct impact on land management practices, economic health and social processes of concern at the national and global level (Dwivedi et al., 2005). However, land degradation has been a threat to natural resources for centuries; inappropriate use of land for agriculture and poor management of its ecosystem coupled with high population pressure lead to environmental problems such as land degradation through accelerated soil erosion and downstream sedimentation (Temesgen et al., 2009).

In addition, FAO (2016) reported that there was a net forest loss of 7 million hectares per year and a net gain in agricultural land of 6 million hectares per year in tropical countries between 2000 and 2010. Lowlands experienced the greatest net loss of forest and a net increase in arable land over this period, an income group in a country with a growing rural population. Sub-Saharan Africa consists largely of agrarian societies relying primarily on low-input agriculture and animal husbandry.

The result is a gradual increase in deforestation and population; forest loss is highest in areas that require wood for fuel or need forest cover and cultivation of crops (FAO, 2015).

2.3. LULC Change Impacts on Hydrology in Ethiopia

According to the various studies carried out in Ethiopia, sub-catchment hydrology is adversely affected by deforestation of natural vegetation, soil degradation, and agricultural expansion. This reduces infiltration groundwater recharge and increases runoff (Dwivedi et al., 2005; Kuma et al., 2023; Woldemariam & Harka, 2020). The study done in the Melka Kuntrie sub-basin located in the Upper Awash River Basin by Getahun & HAJ (2015) has shown that there is higher drainage in major rivers due to high deforestation and

evapotranspiration.

This means that there have been fluctuations over time change in river discharge due to land use land cover change. Also, in the study done in the Erer-sub basin in the Wabe-Shebelle River basin, there was observed a decrease in the water body this is due to the expansion of the settlements and cropland (Woldemariam & Harka, 2020). Changes in land use/cover have a particular impact on the catchment's sediment production and the flow available for ecosystem function as well as human use. Therefore, LULC alteration maylead to a decrease in the availability of a number of products and services for humans, animals, and agricultural production, which may also affect the environment.

More studies need to be done on this Wabe-Shebelle River basin to assess the impacts of this LULC dynamics. Therefore, this study will have the objective of detecting land use and land cover change impacts on the water balance component of the Gobele watershed in the Wabe Shebelle River basin using satellite images acquired in different years. Land use thus includes both the manner in which the biophysical properties of the land are manipulated and the intent (for which the land is used, e.g. agriculture, grazing, etc.) that emphasizes that manipulation; these are more subtle changes that can influence the nature of the land cover without changing the overall classification.

2.4. Remote Sensing Application in Land Use Land Cover Change Analysis

Remote Sensing (RS) technology is used to detect changes in land cover in many areas of Ethiopia. Remote sensing (RS) integrated with geographical information systems (GIS) provides powerful tools for analyzing land use and land cover change.

By using multi-temporal images with GIS modelling, land use land cover change detection comes up with good and interpretable results. Change detection is useful in many applications related to land use and landcover (LULC) changes, such as shifting cultivations and landscape changes, forest degradation and desertification (Halefom & Teshome, 2018). Remote sensing and GIS were applied in different parts of Ethiopia in land use land cover change detection; Tolosa (2018) applied remote sensing and GIS to assess land use and land cover studies on the dynamics of the upper Blue Nile basin show that forests and shrubs are decreasing, while farmlands and grasslands are increasing. This change was due to the increase in human livestock in this area. Satellite remote sensing is widely used in

conjunction with geographic information systems (GIS).

It is recognized as a powerful and effective tool for detecting changes in land use and land cover. Satellite remote sensing provides cost-effective multispectral and multi-time data. It transforms it into valuable information to understand and monitor land development patterns and processes to create long-term land use and land cover datasets.

Predicting future land use and land cover is current research with great benefits for urban planning and natural resource management. Modeling of LULC change is a rapidly growing scientific field these days. Many modelling tools are used, and LULC change models can be fundamentally different in many ways, making it difficult to compare the performance of different modelling tools. Among the many tools and techniques for modelling land use and land cover, the most commonly used models are Cellular Automata (CA) Markov, Markov Chain, GEOMOD, etc. TerrSet software's land change modeller uses a CA-Moakov chain-based neural network to predict his LULC in the future (Kusuma et al., 2016).

Gobele watershed is undergoing rapid land use transformations due to various socioeconomic and environmental factors, such as population pressure, agricultural development, deforestation, and urbanization (Woldemariam & Harka, 2020). So, it is essential to evaluate theimpacts of LULC and climate change on water balance components in the watershed.

2.5. Climate Change Overview

Scientific researchers in different sectors look for evidence for climate change detection by exploring historical records, collecting measurements, and observing temperature trends, weather patterns, sea level, and other environmental features (Getachew et al., 2021; Legg, 2021), Climate change is already happening today and causing so many problems.

Climate change can be defined as a shift in the climate's condition that lasts for a long time, usually decades or more. It may be detected (for example, by statistical tests) by changing in the mean and variability of its attributes. This change can be due to natural variability or human activities. The sun's energy is the main driving force of the climate system. Total solar radiation is balanced by an equal amount of radiation returning to space to maintain a temporary balance between incident and reflected solar radiation. However, this balance can be disturbed, disrupting the climate system. These can be separated into two processes: external and internal (IPCC, 2007). The variation of climate change by natural or human activities affects precipitation intensity, amount, frequency and type; as a result, it leads to

environmental degradation and loss of human life due to its association with flood and drought (Trenberth, 2011). General changes in the global climate aresometimes very rapid.

The global average temperature has been rising since the 20th century due to greenhouse gas emissions (Ritchie et al., 2020). This changing pattern of temperature leads to climate change, which has devastating effects on natural resources and human beings. The main greenhouse gases (GHG) are carbon dioxide, methane gas, and nitrous oxide (IPCC, 2014). However, the main reason for concern is the speed at which human activity is taking place, releasing additional amounts of these gases, including more potent halocarbons (Miller et al., 2014).

The IPCC 5th Assessment Report (AR5) concluded that the observed rise in anthropogenic greenhouse gas concentrations since the mid-20th century is most likely responsible for the majority of the observed increase in the global average temperature and, as a result, leads to drought hazards (Ritchie et al., 2020).

2.5.1. Cause of Climate Change

Climate change is caused by a change in greenhouse gas concentration due to natural and anthropogenic forcing, but anthropogenic is the main source of greenhouse gases. Carbon emissions and other greenhouse gases in the atmosphere are rising as a result of human activities such as the use of fossil fuels, their manufacture, agriculture, and changes in land use. These emissions can alter the planet's climate. Carbon dioxide is one of the main greenhouse gasesthat are important to the Earth's energy balance (Thuiller, 2007).

2.5.2 Change of Climate in Ethiopia

Ethiopia is a country in the Horn of Africa that is roughly 1.2 million square kilometers in size. It has mountains and the wide variety of climatic conditions, wildlife, ethnic groups, and cultural practices. Its weather can be hot and dry or cold and humid. In comparison to most of Africa, the nation is also blessed with abundant water resources. The sustainable development of these natural resource bases is still pending for the nation's socioeconomic advancement. Although there have been few quantitative evaluations of how climate change is affecting different socioeconomic sectors in the nation thus far, it is anticipated that these consequences would be negative on an ecological, social, and economic level (NAPA, 2007). The study done on Melka Wakena in the Wabe Shebelle River Basin indicated that for both

future periods under both scenarios, mean annual precipitation is expected to decrease over the study area.

However, mean monthly variations will be higher than annual variations. The monthly simulated rainfall under RCP8.5 was expected to be larger than under the RCP4.5 scenario in March and April. However, the annual reduction trend is significant for the RCP4.5 scenario (Fita & Abate, 2022a).

The study also noted that the minimum temperature is increasing at a higher rate than the maximum temperature. Moreover, the International Panel on Climate Change (IPCC) Fifth Assessment Report found that recent reports from the Famine Early Warning Systems Network indicate that there has been an increase in seasonal mean temperature in many areas of Ethiopia. Different studies performed in Ethiopia showed frequent increases in temperature, which will make the country hot over time (Fentaw et al., 2018; Orkodjo et al., 2022).

There are various studies done in different Ethiopian river basins to evaluate the impact of both land use land cover and climate change on water balance components, but there is a gap in Wabe Shebelle River Basin; there are no thorough studies to assess the existing condition of land use land cover as well as climate change and to make their forecast in order to introduce the mitigation and adoption to climate change; so this study will play a great role in filling this gap by analyzing the land use/ cover and climate change impact on water balance components in GobeleWatershed in Wabe Shebelle River Basin.

2.5.3. Climate Change Impacts on Water Balance Components

Changes in the characteristics of water balance components due to climate change depend on individual aspects of the water body. The effects of climate change on stream flows, evaporation, water volume and other hydrological parameters are mainly related to the prediction of climate variables (e.g., precipitation, temperature, humidity, mean sea level pressure) on a global scale.

Variations in the primary climate variables are associated with significant repercussions of climate change, which will subsequently result in modifications to the type of land cover, vegetation, and hydrological regime (Shiferaw et al., 2018). Variations in temperature and precipitation were set up influential in stream flow trends in colorful regions across Ethiopia (Orkodjo et al., 2022).

Wind and temperature variations have an impact on the sub-processes of transpiration and evaporation, which in turn affect the budgets of surface and ground water (Zhang et al., 2016). Gizaw et al. (2017) assessed the impact of climate change on the stream flow of four major river basins in Ethiopia: Baro, Awash, Genale, and Tekeze; the ensemble mean of 10 GCMs show the increase in temperature in the areas by 2.3 °C and 3.3 °C in the 2050s and 2080s respectively, whereas the mean annual precipitation is projected to increase by about 6% and 9% in 2050s and 2080s respectively. This increase in precipitation results in a 3% and 6% increase of the projected annual stream flow in Awash, Baro, and Tekeze rivers, whereas the annual stream flow of Genale River was projected to increase by 18% and 33% in the 2050s and 2080s respectively. On the other hand, the declining trends in mean annual precipitation seen in recent decades are at odds with the projected increase in mean annual stream flow brought on by increased precipitation over Ethiopia.

Precipitation is the source of water in the watershed, and the available water is the difference between precipitation and loss, which is called evapotranspiration. Available water contributes to surface runoff and stream flow. Thus, increased precipitation may lead to an increase in surface runoff, while a drop in precipitation can affect the contrary effects. Increasing temperature in Ethiopia's Lake Ziway watershed impacted hydrological processes by raising evapotranspiration (Hordofa et al., 2022). Runoff decreased by over 18% to increase evapotranspiration by 30%on selected catchments in the Blue Nile basin (Chimdessa et al., 2018).

2.6. Climate Modeling

2.6.1 Types of Climate Models

Climate models, both global and regional, are the primary tools that aid in our understanding of the many processes that govern the climate system (Pal et al., 2007). Climate change is one of the most challenging geophysical systems to simulate, and it will have a direct impact on the availability and variability of freshwater as the frequency of climatic extremes such as heat waves, drought, and changes in the rainfall pattern increases in response to global warming.

Since they aim to reflect the primary elements of the climate system in three dimensions, global climate models, also known as general circulation models (GCMs), are the most

complicated of all climate models. Many studies claim that GCMs are an essential tool for conducting climate change experimentson a regional, global, and extremely small scale up to a specific climate pattern from which climate change scenarios are formed (Ahmed et al., 2013). However, their course resolution is one of their key weaknesses. The majority of the time, they do not produce the most crucial statistical characteristics, such as mean and variance, for the current climatic trend (Hordofa et al., 2022).

The resolution of a regional climate model (RCM) is higher than that of a global climate model (GCM). To enable more in-depth simulations for a specific place, it can be layered within a global model. Local topographical characteristics, such as mountains, have a significant impact on local climate ‘change. GCMs do not capture small-scale topographical 12 details because of their poor resolution. RCMs are impacted by smaller-scale topographical factors and have a better resolution than a GCM (25 km). Running an RCM requires substantially more processing power; hence, they are often conducted only over a small region (Ahmed et al., 2013). The Coupled Model Intercomparison Project (CMIP) is dedicated to generating standardized climate simulations for use by various scientific communities, taking into account the time that different versions of GCMs have been produced (Collazo et al., 2022).

In order to gain a better understanding of climate variability through a series of carefully planned experiments, a new generation of CMIP-GCMs has just been designed for phase six CMIP6 experiments, updated emission, concentration, and land use scenarios (SSPs) marked the beginning of the CMIP6 (Du et al., 2022). Rather than the high resolution, The start years for the future scenarios and the new sets of concentration, emission, and land use specifications data are additional distinctions between the CMIP6 simulations and the earlier CMIP phases (CMIP3 and CMIP5) (Shiru & Chung, 2021). The CMIP6 scenarios (SSPs), which are based on eight scenarios, account for projected changes in the Earth's climate in addition to global economic and demographic developments. The SSPs of concern include SSP1-1.9, SSP1-2.6, SSP2-4.5, SSP3-7.0, SSP4-3.4, SSP4-6.0, SSP5-3.4, and SSP5-8.5 (Rhymee et al., 2022). The scenarios with the same radioactive forcing as the CMIP5 scenarios of RCP 2.6, 4.5, 6.0, and 8.5 are SSP1-2.6, SSP2-4.5, SSP4-6.0, and SSP5-8.5 (Wainwright et al., 2021).

Therefore, the CMIP6 models better capture the physical properties of the planet, and their scenarios enable a more realistic evaluation of the effects of climate change policies. The

CMIP6 dataset indicates more serious warnings and intense projections because it is more sensitive to extreme climatic factors (Collazo et al., 2022).

2.6.2 Climate Change Scenarios

Since the 1970s, climate scenarios have played a significant role in global change research as a way to describe uncertainty in intricately interconnected human and natural systems. They are used to investigate how various potential future scenarios may develop, as well as how desired results might be attained and unfavorable consequences avoided. By offering a limited number of common climate change and social futures for use across research communities, they have contributed significantly to the study of global change (O'Neill et al., 2020). Climate scenarios are widely considered a key tool for climate change impact and risk assessment. Previously, Special Report Emission Scenarios (SRES) were developed by the IPCC in the 1990s (IPCC, 2014).

It developed from storylines that were used in climate change research and assessment, and theyare based on population, technology, energy, and land use as driving forces. Since 2010, a number of communities have worked together on the so-called Shared Socioeconomic Pathway (SSP)-Representative Concentration Pathway (RCP) framework, which includes a number of different socioeconomic development pathways (SSPs) and atmospheric concentration pathways (RCPs) with corresponding climate change outcomes (Moss et al., 2010).

The RCPs were published in 2011 and are based on the multi-model ensemble of CIMP5. They are better at identifying the climatic convergences of nursery gases in environmental change convection and advancing comprehension of the conceivable environment and future financial turnof events. The SSPs were published in 2017, which is based on the multi-model ensemble of CIMP6; it is a new set of scenarios that have been created to describe likely pathways for various emanations and financial circumstances and to evaluate cultural capacities to address moderationand adaption difficulties (O'Neill et al., 2020).

2.6.3. Downscaling Techniques

Downscaling is a term that has been used to describe various methods used to derive regional or local scale climate data from coarsely resolved climate models (Schoof, 2013). The hydraulic effects of environmental change are normally surveyed by downscaling the Global Climate Model (GCM), which results in huge scope environmental factors to regional

scale hydrologic factors.

Such an evaluation is described by vulnerability coming about because of the troupes of projections produced with various GCMs, which is known as intermodal or GCM vulnerability. In fact, GCMs are important prescient instruments. However, they cannot give good data about fine-scale heterogeneity and environmental change because of their coarse goal. As the scene highlights, parts of the environment framework have scales that are better than 100km (Ghosh & Mujumdar, 2009).

Furthermore, due to coarse spatial resolution, climate models are characterized by uncertainty to simulate local scale climate variables that are used as input in hydrological models, and then downscaling is recommended. Downscaling approaches are the tools used to obtain fine-scale climate information from the coarse GCM.

For the most part, there are two downscaling procedures: dynamical downscaling and statistical downscaling. Dynamic downscaling is one of the methods that move data from GCMs to the fine-scale by applying a higher-goal RCM over a restricted region with introductory and limit conditions taken from a driving GCM; statistical (empirical) downscaling methods are based on the existing relationships between large scale variables and local variables (Walton et al., 2015).

Statistical downscaling methods have been widely applied in adaptation and impact studies dueto their low computational cost and low time compared with dynamic downscaling.

2.6.4. Bias Correction Approaches

Bias is defined as the systematic difference between a modelled property of the climate system and the corresponding real property. Such properties can be mean temperature, variance, or 100-year return value (Maraun et al., 2017). Bias correction is based on reference data for observations that should, in many cases, be considered a sample product. The reason behind the bias correction is to identify the possible mismatches between observed and simulated climate variables underlying both regulation and scenario correction climate models (Ghosh & Mujumdar, 2009).

The sources of biases are systematic model errors due to imperfect conceptualization, discretization, and spatial averaging within grid cells. The bias correction methods are stationary by assumption, i.e., the correction algorithm and its parameterization for current

climate conditions will continue for future conditions (Maraun et al., 2017) that the scientists established the different means of bias correction by downscaling the environmental factors from models' reach, and from straightforward scaling ways to deal with additional complex generators.

It is vital to distinguish a proper bias correction technique and apply predisposition revision to environmental model simulation prior to utilizing environment models in different applications. Inthis study, distribution mapping embedded in the Cmhyd tool was used in the bias correction of precipitation and temperature data (Chen et al., 2013).

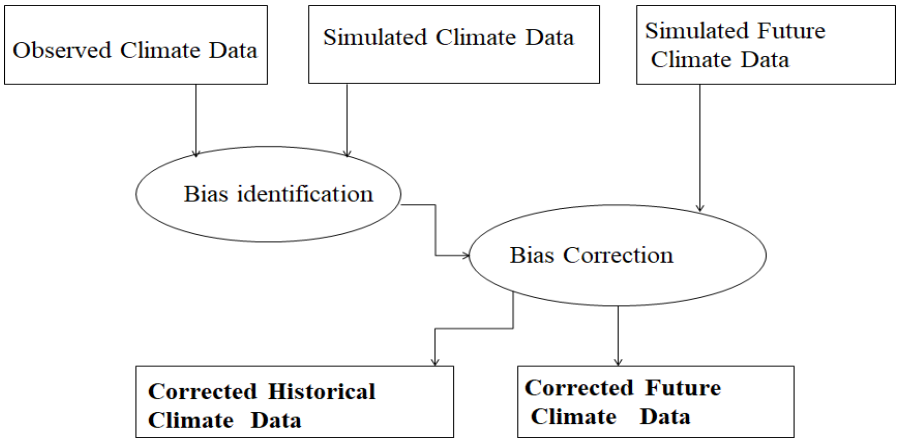

Figure 2.2 Bias correction procedures

2.6.5 Comparison between CMIP5 and CMIP6

The Coupled Model Inter-comparison Project (CMIP) is resolved to give normalized climate simulations for the utilization of various researchers. CMIP5, which is phase five with its inserted GCMs and experiments, is complex and has low resolution. They cover a more extensive scope of scientific issues utilizing a few Representative Concentration Pathways(RCPs), which are RCP 2.6 (Low emissions), RCP 4.5 (Medium emissions) and RCP 8.5 (high emissions) (Taylor et al., 2012).

Recently, a new generation of CMIP GCMs has been developed for phase six CMIP6 experiments with the purpose of getting a deeper understanding of climate variability by conducting a series of well-coordinated experiments. CMIP6 models have higher spatial resolution and improved parameterization schemes for key physical and biogeochemical

processes in the climate system as compared to CMIP5 models' output (Wainwright et al., 2021).

CMIP6 is the improved coupled models that consider emissions, social economic condition and land use scenarios that are known as Shared Social economic Pathways (SSP). The SSPs in CMIP6 take into account future changes in the Earth's climate as well as the world's economic and demographic trends based on eight scenarios. SSP1-1.9, SSP1-2.6, SSP2-4.5, SSP3-7.0, SSP4-3.4, SSP4-6.0, SSP5-3.4, and SSP5-8.5 are the SSPs in concern while for CMIP5 is concerned with RCP 2.6, 4.5, 6.0, and 8.5 scenarios that are having the same radioactive forcingwith SSP1-2.6, SSP2-4.5, SSP4-6.0, and SSP5-8.5 scenarios of CMIP6.

The CMIP6 phase's goal is to overcome and enhance the limitations noted in the CMIP5 output, namely finding systematic simulation mistakes and enhancing the representation of how changes in land use affect climate (Rhymee et al., 2022). CMIP6 models have shown subjective and quantitative improvement contrasted with the CMIP5 models, high spatial resolution, simulated fields, and the display of physical processes. In comparison to CMIP5, CMIP6 has lower error coefficients and better correlation, which suggests stronger predictions and more serious warnings.

2.6.6. Homogeneity Test and Trends Analysis

For progressively more advanced investigations of climate change, the homogeneity test and trend analysis of temperature and rainfall are essential (Bisai et al., 2014). The relocation of the meteorological station, malfunctioning meteorological equipment, improper data handling, and sudden climatic changes are the main causes of the non-homogeneity in the observed data (Getahun et al., 2021). Potential causes of non-homogeneity in future climate data include shortcomings in bias correction techniques. The Buishand's range (Che Ros et al., 2016), standard normal homogeneity (SNH), Pettit's range test (Pettitt, 1979), von Neumann ratio (VNR), Mann-Kendall test, Sen's slope, and other methods are used to analyze the change in hydro-climatic variables, both seasonal and annual trends. The Mann-Kendall test is a nonparametric technique that works best with independent data and is less sensitive to outliers (Hamed, 2008; Toni et al., 2022). Furthermore, Mann-Kendall includes a tall degree of unwavering quality for finding monotonic patterns in climate time arrangement information; in this way, the nonparametric MK strategy has been broadly utilized to find

patterns in hydro-meteorological time arrangement information and is, as a rule, advanced by the World Meteorological Organization (Ali et al., 2019; McLeod, 2005).

2.7 Hydrological Modeling

A model is a condensed representation of a system in the actual world. The best model is the onethat produces results that are midterm to reality while utilizing the fewest parameters and the least amount of model complexity (Talebmorad & Ostad-Ali-Askari, 2022). Models are primarily used to analyze various hydrological processes and anticipate system behavior. It describes the interactions between the many hydrological processes, such as stream flow, infiltration, evaporation, and rainfall, which changein time and place (Access et al., 2008).

By utilizing the models, we are able to understand how the water balance components are affected. They can be applied to foresee potential results of not only historical and present but also future situations, so assisting in the development of solutions to real-world issues with a level of detail that is not achievable with traditional pen-and-paper research.

In hydrology, it is also crucial since it is difficult and impracticable to physically observe the interactions above at a sufficient number of places across the watershed. Furthermore, any potential alterations to the hydrological system, such as those brought on by human activities, need to be identified far sooner so that suitable mitigation measures may be putin place.

As a result, modelling is the sole method for swiftly predicting the future and figuring out what will happen if current circumstances remain the same, get better, or get worse (Singh et al., 2015). Based on the process description, hydrological models can be classified into three categories: lumped models, semi-distributed models, and distributed models (Singh, 2018).

Distributed models are the most complex as they account for spatial homogeneity of inputs and parameters. Fully distributed models separate the model process into small grid cells; each grid cell has its hydrological response calculated separately. For example, some of the physical distributed Models, MIKESHE and VELMA.

Semi-distributed models are a variation of lumped models with features and distribution models. They have parameters that are partially distributed in space by dividing the basin into sub-basins. Among them we have HEC-HMS, TOPMODEL, and SWAT.

Lumped models take the river basin as a single homogenous unit, and the spatial variability of the river basin parameters is disregarded. Normally, a lumped model is designed to

simulate total runoff and stream flow at the outlet point, not specific flow within the basin. For example, Empirical and conceptual models, machine learning.

2.7.1 Hydrological Model Selection

There are a range of possible model structures within each class of models. Hence, choosing a particular model structure for a particular application is one of the challenges of the model usercommunity. The following are the suggested criteria for selecting model:

1. Consider models which are readily available and whose investment of time and money appeared worthwhile.
2. Decide whether the model you are considering will provide the outputs needed to achieve the specific project goals.
3. Prepare a list of assumptions made by the model and check the assumptions likely to be limiting in terms of what is known about the response of the catchment. This evaluation is usually relative or, at best, involves rejecting models based on patently false representations of the catchment processes.
4. Make a list of the inputs required by the model and decide whether all the information required by the model can be provided within the time and cost constraints of the project (Beven, 2001). Thus, a semi-distributed physically based hydrological model SWAT was selected for this particular study by considering the factors stated above, and it is a basin-scale model used to simulate land use land cover map of different periods and rainfall- runoff to predict the future climate change and LULC change impacts on surface hydrological processes in Gobele watershed.

2.7.2. SWAT Model Description

SWAT stands for Soil and Water Assessment Tool, it is Soil water assessment tool (SWAT) is a continuous time, spatially distributed model developed for the USDA Agricultural Research Service (ARS) designed to simulate water, sediment, nutrient and pesticide transport at a catchments scale on daily time step, monthly or even annually (Sisay et al., 2017). SWAT model has recently received recognition on a global scale as a reliable trans-disciplinary watershed modelling tool (White & Chaubey, 2005).

It makes use of hydrologic response units (HRUs) that have particular slope, soil, and land

use characteristics within a watershed; geographical variability in terms of land cover, soil type, and slope class is described using HRUs. HRUs unit, the model calculates pertinent hydrologic elements, including evapotranspiration, surface runoff and peak runoff rates, groundwater flow, and sediment output. A GIS interface has a SWAT embedding. An ArcView extension for an older version of SWAT, AVSWAT, evolved into Arc-SWAT ArcGIS extension, which providesa graphical user interface for SWAT (Arnold et al., 2012; Fentaw et al., 2018; Mitiku et al., 2023).

Numerous studies support the SWAT model's applicability to circumstances in Ethiopia at various topographic, watershed, and basin scales. They also evaluate the effects of climate change on hydrology as well as LULC dynamics (Chaemiso et al., 2016; Fita & Abate, 2022a; Kenea et al., 2021; Shigute et al., 2022). All these researchers indicated that the SWAT model is capable of simulating hydrological processes with reasonable accuracy; as the SWAT model is semi-distributed, it divides a watershed into various sub-watersheds, which are then divided into hydrological response units (HRUs) consisting of homogeneous land use, management and soil properties (Alemayehu et al., 2017).

The SWAT model, like other hydrological models, has some uncertainty that it requires calibration for the reduction of the uncertainty, so SWAT-CUP (Calibration and Uncertainty Program), R-SWAT and other software have been developed to perform this function (Healy & Essaid, 2012). The above software contains a series of procedures used for calibration and validation of the models, such as particle Swarm optimization, Generalized Likelihood Uncertainty Estimation (GLUE), Parameter Solution, Markov Chain Monte Carlo, and Sequential Uncertainty Fitting Ver.2 (SUFI-2).

The assessing the impact of climate change on surface hydrological processes using SWAT was based on the hydrologic cycle water balance equation:

$$SW_t = SW_0 + \sum_{i=1}^{t}\left(R_{day} - Q_{surf} - E_a - W_{seep} - Q_{gw}\right) \quad (2.1)$$

Where SWt is the final soil water content (mm), SWo is the initial soil water content on day I (mm), t is the time (days), Rday is the amount of precipitation on day I (mm), Qsurf is the amount of surface runoff on day I (mm), Ea is the amount of evapotranspiration on day I

(mm), Wseep is the amount of water entering the vadose zone from the soil profile on day I (mm). Qgw is the amount of return flow on day I (mm).

Surface runoff is calculated in the SWAT model using either the Soil Conservation Service Curve Number (SCS-CN) approach or another method (USDA-SCS). SCS-CN will be used to conduct this research. The SCS curve number isdescribed using the following equation:

$$Q = \frac{(P - I_a)^2}{(P - I_a) + S} \quad (2.2)$$

Where Q is the depth of runoff in (mm), P is effective precipitation in (mm), Ia is the initial abstraction of water in (mm), and S is maximum potential retention. However, the initial abstraction ofwater (Ia) is the function of maximum potential retention S.

Therefore, Ia =λS where λ=0.2 and Ia =0.2S the equation becomes

$$Q = \frac{(P - 0.2S)^2}{(P - 0.8S)} \quad (2.3)$$

When P is higher than 0.2 S, runoff processes take place. Because of this, the potential retention parameter changes according to the soil types, catchment slope, and land use management. The following equation connects the dimensionless parameter CN and the greatest possible retention of S.

$$S = \frac{(25400}{CN} - 254) \quad (2.4)$$

The soil's permeability, infiltration, land use, and soil-water conditions all affect the SCS curve number (CN). Three circumstances may be used to determine the CN value: dry, average moist, and wet. Surface runoff, runoff, evaporation, catchment storage, reservoir water balance, deep aquifer, and infiltration are among the created and validated outputs of the SWATmodel.

2.8 Literature Review of Previous Similar Studies

The most dangerous problems in the world now are those related to climate change as well as land use and land cover change. Climate change's effects on water supplies are a global concern.

Moreover, LULC change is increasing due to overpopulation, rapid urbanization, and land expansion in agriculture. Due to this remarkable change, numerous scientists have been

analyzing the effects of climate change and land use, including land cover change on water resources and the river basins' hydrological processes. As the study area is in Ethiopia, the related studies done in the Ethiopian river basin with their gaps, especially in the Wabe Shebelle river basin, where the Gobele watershed is located, are discussed below.

Mitiku et al. (2023) used climate models from CORDEX-Africa RCM based on RCP4.5 and RCP8.5 scenarios in CMIP5 and the SWAT hydrological model to examine the impacts of climate variability and land use change on hydrological responses of Awash River basin, Ethiopia, the objective of the study was to diagnosis the influences of climate and land use changes on hydrological responses of upper Awash River.

The results show that the stream flow will increase in all scenarios, and climate change effects on the stream flow basin are more pronounced than the influence of LULC change. In addition, precipitation and temperature have shown an increasing pattern over the study period. The gap from this study is that the climate emissions scenarios used were different from the latest version.

Fita and Abate (2022) used a Soil Water Analysis Tool (SWAT), and based on RCP4.5 and RCP8.5 scenarios in CMIP5, they assessed the impact of climate change on the stream low of the Melka Wakena reservoir in the Upper Wabi Shebelle sub-basin. The result shows an expansion in extended least and greatest temperatures under RCP4.5 and RCP8.5 environment situations; also, precipitation will decrease. Gurara et al. (2021) investigated the impact of climate change on the potential evapotranspiration and crop water requirement in the Upper Wabe Bridge watershed, Wabe Shebele River Basin, Ethiopia, by using CORDEX-Africa RCM climate models based on RCP 4.5 and RCP 8.5 scenarios in CMIP5 and the SWAT hydrology model (Woldemariam et al., 2018).

The results show the increases in temperature and PET in all scenarios, and crop water requirement did not change significantly from one station. Getahun & Haj (2015) used remote sensing and Soil Water Analysis Tool (SWAT) to evaluate the spatiotemporal trends of land use and land cover changes over the last four decades and to identify the effects of land degradation/land use and land cover change on sediment yield in Melka Wakena Catchment. The results show increases in the surface runoff from 1990 to 2010, whereas decreased until 2013.

The current climate model version, CMIP6, was not applied to those earlier, comparable studies to analyze the effects of climate change and in all those studies, they did not consider the land use land cover change prediction except in the study of Mitiku et al., (2023) which considered the LULC prediction in future time, where they reported the increases in both agriculture and built-up area.

However, previous studies have yet to perform change-point detection tests on future climate data in the Gobele watershed. This shows that the Wabe Shebelle basin, in general, still needs an in-depth understanding of the quality of future temperature and rainfall data for different time series, particularly in the Gobele watershed, where this study is focusing.

Moreover, the current research also introduced a climate model with commonly utilized old version scenarios (RCP 4.5 and RCP 8.5), high spatial resolution, and ensemble models. This study further assessed the performance of the climate models ensemble and the better-performing climate models. It introduced the global climate models with the latest version of scenarios (SSP2-4.5 and SSP5-8.5) in CMIP6 and performs the land use land cover prediction in future time.

3. MATERIALS AND METHODS

3.1. Description of the Study Area

3.1.1. Location

This study was conducted in the Gobele watershed, which is located in the Wabe Shebelle River Basin in East Hararghe Zone, Ethiopia. The geographical location of the Gobele watershed extends from 9˚0’0” N to 9˚30’0” N latitude and from 41˚40’0”E to 42˚10’0” E longitude (figure 3.1). The Gobele Watershed has a size of 1627 square kilometers square.

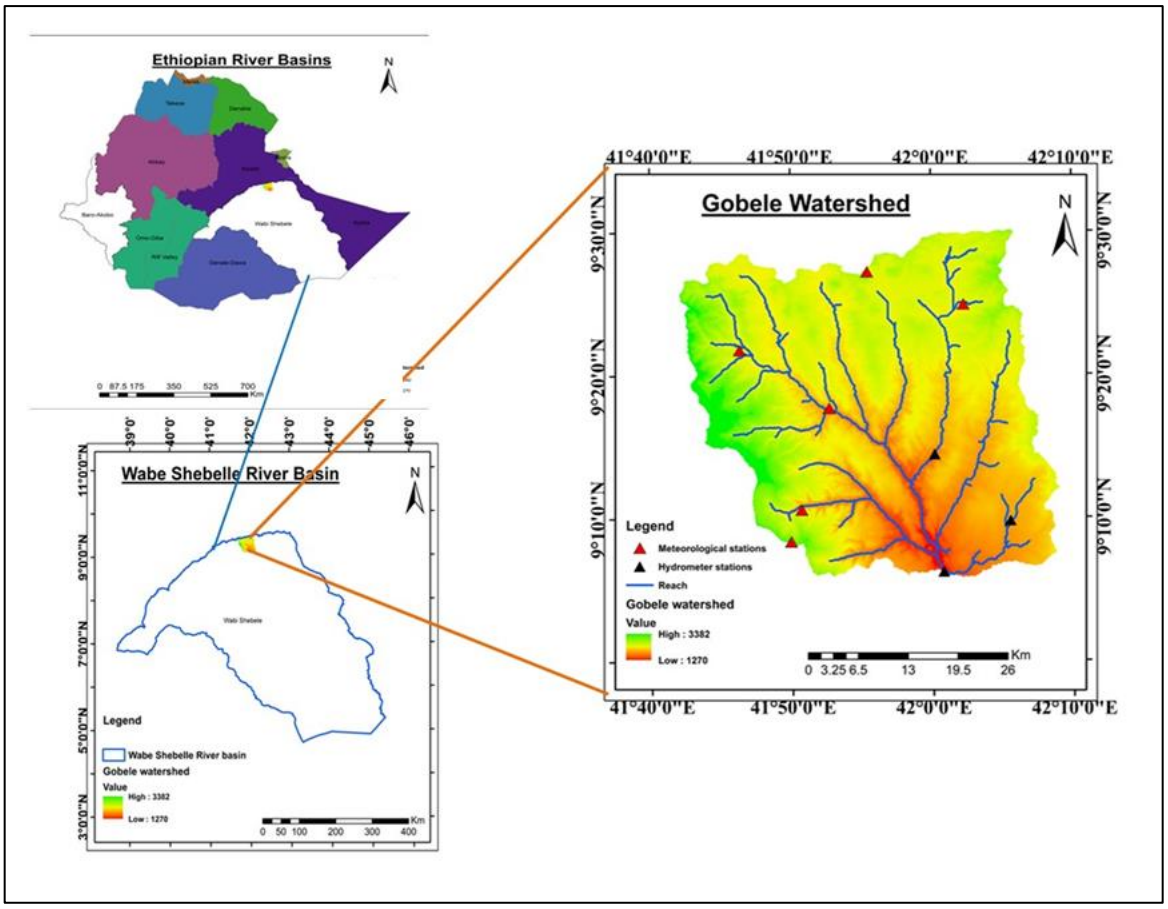

Figure 3.1 Location Map of the Study Area

3.1.2. Topography

Elevation of the study area ranges from 1270 to 3382 m above mean sea level. The topographic features of the watershed are highlands and lowlands. A steep valley on the slopes characterizes the upstream of the watershed, while the lowlands have gentle slopes.

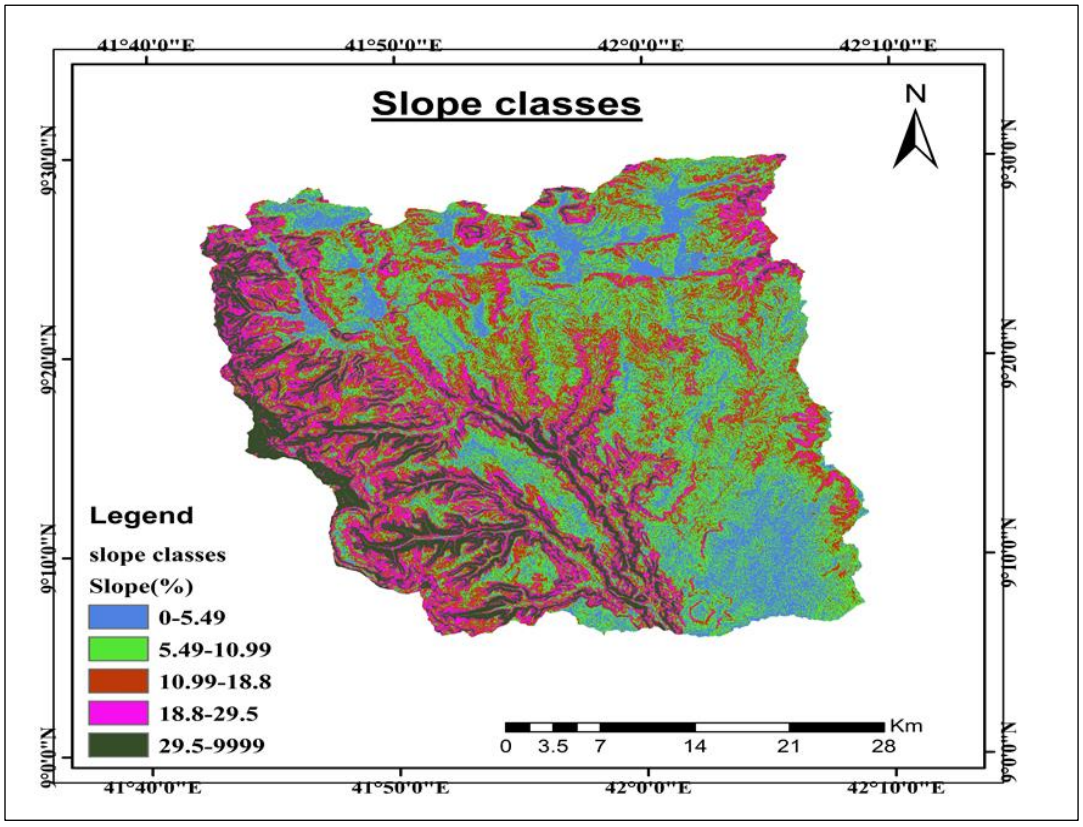

Figure 3.2 Slope Classes of Gobele Watershed

3.1.3. Climate and Hydrology

Gobele Watershed has a tropical climate with both average annual minimum and maximum temperatures ranging from 9 to 17℃ and 21 to 31℃, respectively. The average annual Rainfall from 1990 to 2020 is 1024 mm. The hydrologicalregime in the study area is characterized by factors such as basin surface flow, groundwater recharge rate depending on excess Rainfall, evaporation, soil characteristics and permeability of the bedrock (Woldemariam & Harka, 2020). The monthly rainfall distributions of the study area indicate that July, August, and September are the wettest months of the year.

3.1.4. Soil Types and Land Use Land Cover

The dominant soil types are gypsum, calcisols and leptisols, which cover 68% of the basin. Alarge part of the population in the highlands depends on the cultivation of crops, while the inhabitants of the lowlands tend to be pastoralists (Toni et al., 2022). According to FAO, the soil types in the basin were classified into Dystric Cambisols (Bd), Eutric Cambisols (Be), Humic Cambisols (Bh), and Eutric Nitosols (Ne) (Figure 3.3). The land use land cover of the watershed is grouped into six categories such as grass/ shrub land (RNGB), forest (FRST), agricultural land (AGRL), barren land (BARR), water body (WATR), and settlements(URBN) (Figure 4.2). Previously, grass/brush land and agricultural land were the most dominant land uses, making up 43.78% and 36.19% of the study area, respectively.

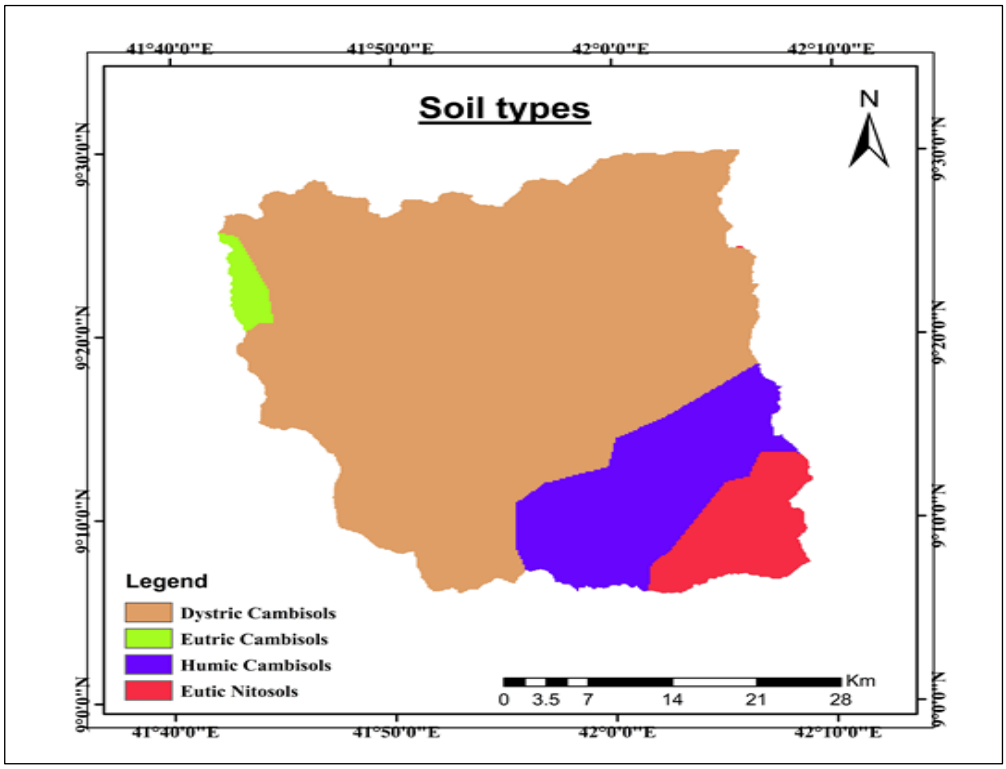

Figure 3.3 Soil Classes of Gobele Watershed

3.2. Data Types and Sources

Spatial data, hydrological and meteorological data were used in this study. The spatial data such as land use maps and Digital Elevation Model (DEM) were downloaded from USGS Earth Explorer. Hydrological data and soil maps were collected from the Ministry of Water and Energy (MoWE). The meteorological data were obtained from the National Meteorological Agency (NMA) (Table 3.1).

Table3.1 Data used in the study and their sources

Data	**Data Sources**	**Purpose**
DEM	Shuttle Radar Topographic Mission: USGS	DEM was used for catchment delineation and elevation map generation.
Soil map	FAO soil classification database	Hydrological Response Unit generation in SWAT model setup
Meteorological data	National Meteorological Agency(NMA)	Future meteorological data forecasting and SWAT model setup
Hydrological data	Ministry of Water and Energy (MoWE)	Calibration and validation of the SWAT model

3.2.1. Meteorological Data

The meteorological data contains daily observed rainfall data, minimum and maximum temperatures, wind speed, relative humidity and solar radiation hours. They were collected from six stations from 1990 to 2020. Both historical (1990-2020) and future (2040-2100) rainfall data, as well as minimum and maximum temperatures derived from observations and four global climate models (GCMs) of CMIP6 through the Earth System Grid Federation (ESGF) gateways that managed, evaluated, and shared model output and observation data.

The CMIP6 output contains global climate metadata in the form of the network command data format (NetCDF), and the data from all four stations were bias-corrected using the Cmhyd tool to improve the water balance simulation in the study area.

Table3.2 Gauged Meteorological Stations in Gobele Watershed

Station name	Latitude	Longitude	Elevation	Recorded years
Alemaya	9.4151	42.0379	2025	1990-2020
Daawe	9.2948	41.8782	1759	1990-2020
Dengengo	9.453448	41.9239	2083	1991-2020
Girawa	9.13952	41.8323	2470	1990-2020
Huse	9.17655	41.3376	1281	1990-2018
Woter	9.36278	41.7722	2020	1990-2020

3.2.2 Hydrological data

The daily observed stream flow data was recorded in the Gobele watershed at the Erer gauging station from 2007 to 2016. The data was checked for consistency using the double mass curve method and continuity using the normal ratio method before being used for further analysis (Figure3.5).

3.2.3. Land Use Land Cover Images

LULC maps of different periods were obtained from Remote Sensing. Cloud-free dry season images of Landsat 4-5 TM (Thematic Mapper), Landsat 7ETM^{+} (Enhanced Thematic Mapper Plus) and Landsat 8 OLI (Operational Land Imagery) were downloaded from USGS Earth Explorer for the years 1990, 2005 and 2020, respectively. The Landsat Level-1 product images were used in this study as these images are terrain-corrected, and the majority of the images can be used as delivered by the USGS (Romañach et al., 2015). Data collections were chosen to be in the dry season to have images with the lowest to zero per cent of monthly cloud cover.

Table3.3 Landsat data information for the study area

Year	Path/Row	Acquisition date	Image	Sensor	Cloud	Resolution
1990	166/054	1990/02/09	Landsat 4-5	TM	3%	30m*30m
2005	166/054	2005/02/04	Landsat 7	ETM+	0%	30m*30m
2020	166/054	2020/01/02	Landsat 8	OLI	0%	30m*30m

3.2.3.1 Images Preprocessing

To reduce errors and enhance the capacity to analyze the image components both qualitatively and quantitatively, preprocessing of the satellite images was carried out prior to classification (Samal & Gedam, 2015). In order to prevent seasonal fluctuations for all images for path and Row, the USGS Earth Explorer provided the Landsat images of Landsat 4-5, Landsat 7, and Landsat 8 for 1991, 2006, and 2020, respectively. The acquisition period was selected in the dry season (January to February) to avoid haze/cloud cover effects.

Using proper band combination in ERDAS software, the images from different bands were combined into a single image to enhance the visibility of the image (layer stacking) as the images were captured from different bands. The combination of different images to cover a large and full region of interest (mosaicking) was not needed as the region of interest in this study was small and could be covered by a single stacked image. Geometric and radiometric corrections are the two main categories of satellite image data correction (Liping et al., 2018). Variations in the pixel intensities (DNs) that are not brought on by the item or scene being scanned are corrected using radiometric correction.

Both geometric correction (topographic normalization) and radiometric correction (periodic noise reduction and haze reduction) were applied to the captured images for this study.

3.2.3.2 Classification

Supervised image classification is a recommended classification approach to yield good results when satisfactory training data and detailed information about the study area are available (Yohannes et al., 2018). A pixel-based supervised image classification with the maximum likelihood algorithm is widely used (Nguyen, 2015), as it has a strong, robust theoretical foundation and can handle a variety of data, LULC types, and satellite systems (Eastman, 2012). In this study, supervised classification was used by employing maximum likelihood classification. In the three periods (1990, 2005 and 2020), satellite images were geo-referenced to the Universal Transverse Mercator (UTM) map projection (Zone 37), WGS 84 datum using a total of 300 ground truth points collected from the

Google Earth for each image.

During the classification, false-color composites were employed to enhance satellite image visual interpretation and make LULC feature detection easier.

3.2.3.3 Accuracy Assessment of Image Classification

Accuracy evaluation was the final stage in classifying and creating maps of LULC. The accuracy was assessed using overall accuracy, user accuracy, producer accuracy, specificity, and the commission and omission errors, as well as kappa statistics from the error/confusion matrix. The accuracy assessment indicates the degree to which the ground truth is reflected on the corresponding classified image. The accuracy results from the classification needs to be evaluated because land use maps that are based on the classification of images typically contain some error.

In order to evaluate the accuracy, Google Earth and ground truth point gathering were used. The ground truth points produced by ArcGIS demonstrate the potential improvement Google Earth can make in confirming the accuracy of categorized images. The link between known reference data (ground truth) and the related outcomes of automated categorization is compared category by category using a confusion matrix.

By dividing the total correct points by the total number of points, the overall map accuracy was calculated. The kind on the ground not found on the classified is the omission error. Pixels that are classified as belonging to one class but were really placed in another are indicated by the percentage of commission. A classified image's thematic accuracy can be examined in a variety of ways. For the classified image, the producer, user accuracy, overall, and Kappa criteria were examined. The equations used to compute different accuracy evaluation indicators are shown below:

$$\text{Producer Accuracy} = \frac{a}{a+c} \tag{3.2}$$

$$\text{User Accuracy} = \frac{a}{a+b} \tag{3.3}$$

$$\text{Specificity} = \frac{d}{d+b} \tag{3.4}$$

$$\text{Commission error} = \frac{b}{b+d} \text{ or } \quad 1\text{-Specificity} \tag{3.5}$$

$$\text{Omission error} = \frac{c}{c+a} \tag{3.6}$$

Where,

a is number of times a classification agreed with the value that was observed, b is the number of times a point was assigned as X classification even if it was not found to be one, c is the number of times a point that was observed to be X was not assigned the X classification, d is the number of times a point was not assigned the classification X even if it was not seento be X, and Total points, $N = (a+b+c+d)$ (Jenness & Wynne, 2007).

$$\text{Kappa Coefficient} = \frac{(TS * TCS) - \sum (TC * TR)}{(TS)^2 - \sum (TC - TR)} \text{x}100 \tag{3.7}$$

Where, TS is the total sample, TCS is the total collected sample, TC is the total columns and TR is the total rows.

According to Mishra & Rai (2016), a kappa coefficient value below 0.4 shows poor agreement, avalue between 0.4 and 0.8 indicates moderate agreement, and a value greater than 0.8 shows strong agreement. Commission and omission error should be ≤ 0.5, both producer and user accuracy should be greater than 0.8 for the strong agreement (Rwanga & Ndambuki, 2017).

3.2.4. Future Land Use Land Cover Images

Based on historical LULC data, future LULC was predicted using the Land Change Modeler incorporated in TerrSet software. The land change model is a mixed model that uses Markov chain and Cellular Automata models. It combines the advantages of a Markov model for long-term forecasting and a Cellular Automata (CA) model to simulate the spatial variation in a complex system (Liping et al., 2018). Different researchers applied an LCM modeler for LULC change analysis and prediction and found that it is more effective as it accurately reflects nonlinear spatially probabilistic land use transformation (Getachew et al., 2021; Kusuma et al., 2016; Leta et al., 2021; Mishra & Rai, 2016).

The LULC transition of 2040 and 2070 was predicted. Prior to predicting the LULC transition in the future, some inputs had to be prepared. The creation of three separate basic land cover maps, which should be used to determine the possibility of transfer and transition suitability, was the first contribution. The second input was factor and constraint map preparation, which allowed for the creation of the necessary image set. Cellular Automata made through the multi-criteria evaluation (MCE) are suitable for all classes and are regarded as a prerequisite. It was adopted for this study as it has shown the best performance in the study of Hyandye and Martz, 2017.

Due to the terrain complexity, societal advancements, and soil and water conservation work regulations, the model requires constraint inputs like Elevation, distance from the road, distance from urban, and distance from the streams to predict the future LULC. The roads were examined using the data collected from OpenStreetMap of Ethiopia; we used them to obtain the distance from the road map, a digital elevation model was used to obtain the elevation map, and a stream map downloaded from DIVA-GIS was used to obtain the distance from the stream map using ArcGIS 10.5.

The constraints were then loaded into the land change modeler to be processed further using the re-class module to convert them into 0 and 1 images. By using a fuzzy module, the future LULC maps were found using a combination of Multi-Criteria Evaluation (MCE) and Weighted Linear Combination (WLC). Finally, to prepare for image collection suitability, each LULC class was grouped using raster group files.

3.3. LULC Classification and Analysis.

Analyzing the catchment morphological characteristics like drainage network, slope divides, and sub-basin boundaries and their responses to land use, land cover, and climate change requires the precondition for hydrological and climate modelling as well as remote sensing. The model inputs were processed in a manner suitable for the SWAT model. The LULC, climate data and soil data of the catchment area are required for SWAT analysis. The Landsat imagery for the years 1990, 2005, and 2020 were processed to find the land use LULC maps.

Weather variables like Precipitation, temperature, relative humidity, sunshine and wind speed data from six meteorological stations were collected from NMA. Some data were missing and were filled using the normal ratio method. Similarly, quality checks for the

stream flow data were done, and the normal ratio method was used to fill in the missing data.

3.4 Hydro meteorological Data Correction

3.4.1 Data Continuity Checking

The continuity of data deals with the absence and presence of the data. Before using recorded meteorological data, it is better to check their quality because some gauging stations might have missing data for different reasons. It is also better to check the accuracy of the available data before use. Filling the missing data and data quality checks are required in order to have good-quality data. The normal ratio method was used to fill in missing data for this study (equation 3.8).

$$P_X = \frac{N_X}{M}\left[\frac{P_1}{N_1} + \frac{P_2}{N_2} + \frac{P_3}{N_3} + ... + \frac{P_M}{N_M}\right] \quad (3.8)$$

Where P_X is the Rainfall at ungagged station X, N_1, N_2, N_3, N_M, and N_X are Normal Rainfall at station1, 2, 3, station M and station X, respectively, while P_1, P_2, P_3 and P_M are the Rainfall at the neighbouring stations.

3.4.2 Homogeneity Test of the Rainfall Data

After filling in the missing rainfall data, the homogeneity of the rainfall gauging station was tested. Homogeneity is a vital issue in identifying the inconsistency of the information. If the information is homogeneous, it implies that the estimations of the information are taken at a time with the same instruments and situations. The application of an inhomogeneous time series to the model can be the source of biases and Uncertainty in the model output. Hence, the homogeneity validation of rainfall data was done by dividing monthly time series data by the average rainfall quantity of the corresponding month. Non-dimensional rainfall data was produced at each station and was used to assess the homogeneity of rainfall gauging stations.

$$P_i = \frac{P_{iav}}{P_{av}} \text{x} 100 \quad (3.9)$$

Where P_i is Non-dimensional value of monthly Rainfall for each station, P_{iav} is Over years averaged monthly Precipitation for the station i, P_{av} is the average yearly precipitation of the station i.

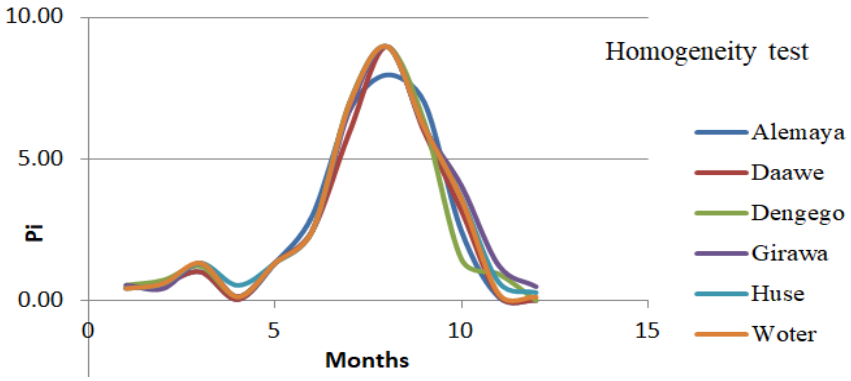

Figure3.4 Non-dimensional Homogeneity Test

3.4.3 Consistency Test of Rainfall Data

If the relevant condition of the recording station has undergone significant changes during the recording period, the recorded rainfall data might show the inconsistency at that station. These changes include moving the rain gauge to a newposition, changes in the environment brought on by harm, deforestation, and impediments and the emergence of observational mistakes starting on a certain date (Bogale, 2015). The double mass curve technique was employed to determine whether a correction was required and to ascertain whether the rainfall data obtained from the Ethiopian meteorological station were consistent across the chosen study period. The double mass curve method is predicated on the idea that recorded data are consistent if they originate from the same parent population.

$$P_X = P_X \frac{M_C}{M_0} \qquad (3.10)$$

Where P_X is the corrected Rainfall at station x, P_x is the original Rainfall at station x, M_c is the original slope of the double mass curve, and M_0 is the collected slope of the double mass curve. To examine whether there needed to be more consistency in gauging stations in the study area, a group of five stations was chosen. The cumulative values of the target stations were plotted versus the cumulative average neighbouring stations using the Microsoft Excel spreadsheet. During the consistency checking, rainfall data showed an inconsistency of 8%, which is very small, so it was ignored, and no correction was needed.

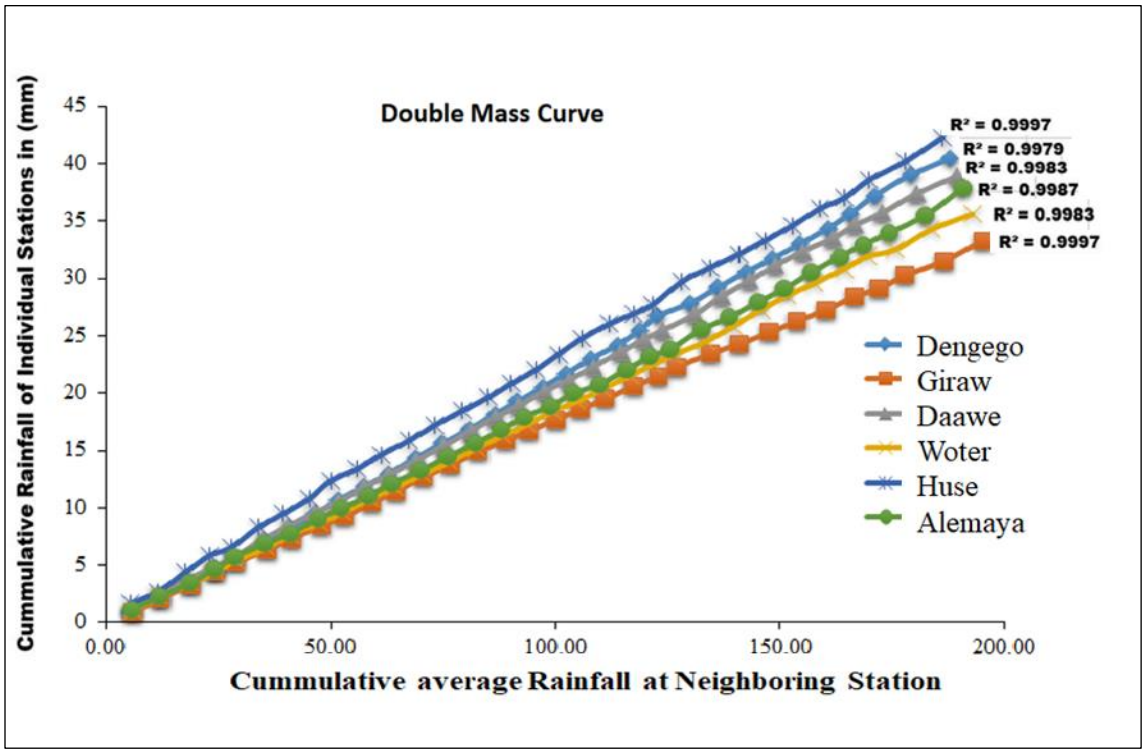

Figure3.5 Consistency check of the rainfall data

3.5 Future climate data

Future climate change is projected to have significant impacts on water resource availability in many parts of the world. In this study, SSP 4.5 as a medium stabilizing scenario and SSP 8.5 as a very high stabilizing scenario were considered. The future climatic data was projected from the new climate dataset project CMIP6 (https://pcmdi.llnl.gov/CMIP6/). This was published as a result of a coordinated effort by many climate research institutes to increase our understanding of and ability to adapt to climate change. The climate impact was estimated using GCMs' daily precipitation and (maximum, minimum) temperature simulations for the historical (1990-2020) and future period (2040-2100) for two SSPs (4.5 and 8.5) collected from the CMIP6 simulation datasets (https://esgf-node.llnl.gov/search/cmip6/).

The output of the climate models covers the years 1985 to 2100 and gives spatial resolution ata global scale between 50 to 250km. SSP1-2.6(low level), SSP3-7.0(middle level), and SSP5- 8.5(high level) are the three Shared Socioeconomic Pathways (SSP)

scenarios used from the CMIP6 archive. Moreover, four climate models and two CMIP6 scenarios (SSP2-4.5 andSSP5-8.5) were used to select the best-performing models in the upper Gobele watershed by comparing their data with observed meteorological data. Seven global climate models were downloaded from CMIP6 (ACCESS-CM2, CNRM-CM6-1, MPI-ESM1-2-LR, ICHEC–EC–EARTH, CSIRO-MK3.6, CanESM2, and CNRM-CM6-1; downscaling of the global climate model to regional scale was performed, and four of the seven model was able to performed well on the Gobele water shed. So they were chosen in this study to analyze climate change impacts on surface water balance components.

Table3.5 Chosen Climate model used in the study and their sources

No	GCMs names	Institution	Resolution
1	ACCESS-CM2	Australian Community Climate and Earth System Simulator	1.25◦ × 1.875◦
2	MPI-ESM1-2-LR	Max Planck Institute (MPI), Germany	1.875◦× 1.875◦
3	ICHEC–EC–EARTH	KNMI Center of the Netherlands	0.44◦×0.44◦
4	CanESM2	CCC ma, Canada	$0.42^0 \times 0.42^0$

3.5.1 Downscaling from Global to Regional Model

Downscaling was done before applying the GCMs data to the hydrological model since theresolution of the GCM-CMIP6 outputs is too coarse for studying the regional future climate change impacts on the hydrological components impact assessment.

The methods used to extract fine-resolution climatic data from the coarse GCM are known asdownscaling (Walton et al., 2015). There are two commonly used downscaling methods: dynamical and statistical downscaling. In this study, the statistical downscaling method was used as it was found to be cost-effective and efficient, allowing a wide variety of transmission scenarios and GCM pairs and having high spatial resolution (Ahmed et al., 2013).

During the downscaling operations, statistical downscaling also determines the statistical relationship between the large-scale (predictors) and local-scale (predictand) climate variables. Variables with a prediction skill for a particular predictor are called predictors (Wilby & Dawson, 2013). Large-scale climate variables obtained from the four

(ACCESS-CM2, MPI-ESM1-2-LR, ICHEC–EC–EARTH, CanESM2) CMIP6 climate models outputs for historical and future climate scenarios, SSP2-4.5 and SSP5-8.5 was in the network command data format (NetCDF), they were extracted and downscaled using Climate Model Hydrological modelling data tool (CMhyd) tool (Rathjens et al., 2016).

3.5.2 Bias Correction of the Future Climate Data

Before being used for additional analysis, the bias in the GCM and RCM model output must be corrected using the suggested techniques because it hinders the research on climate change (Teutschbein & Seibert, 2013). To minimize biases in climate model outputs, there are several methods used that are embedded in the CMhyd tool; among them, we have linear scaling, delta change correction, precipitation local intensity scaling, power transformation of Precipitation, variance scaling of temperature, and distribution mapping (quartile mapping) of Precipitation and temperature.

To carry out this study, distribution mapping was used due to its best performance compared to the others in many studies, and it adjusts the standard deviation and the percentiles while linear scaling does not (Fita & Abate, 2022). The correction method was applied by comparing the daily observed Precipitation and temperature at each station with the nearest grid point of RCM, considering the grid points to be a single station on the watershed.

3.5.3 Multi-Model Ensemble for Climate Change Projection

Based on its applicability in earlier climate change research, the multi-model ensemble mean of four CMIP6-GCMs was calculated using the simple arithmetic mean method of the multi-model ensemble approach (Hemer et al., 2013; Li et al., 2021). The performance of the multi-model ensemble mean was checked over the Gobele watershed for both downscaled and bias-corrected climate models by using observed and historical monthly rainfall maximum and minimum temperatures from 1990 to 2020. Table 3.6 shows the statistical indicators used to validate the performance of the climate multi-model mean at all six stations by using Excel.

Table3.6 Statistical indicators used to evaluate multi-model ensemble of climate models

Indicators	Description	Range	Targeted value
R^2	The relationship between observed data and Ensemble output	[-1,1]	1
RMSE	Indicate the mean magnitude of the error	[0,∞[	0
PBIAS	Measure the mean trends of the ensemble outputs	]-∞, ∞[	0

3.5.4 Trends Analysis of Simulated Climate Data

The rainfall series in each station were examined for trends to determine the potential existence of temporal tendencies; the Mann-Kendall (MK) nonparametric test and Sen's slope were used to determine the statistical significance of these trends (Hamed, 2008; McLeod, 2005). Nonparametric tests were chosen because they are less susceptible to outliers and perform better with independent data than the parametric method (Hordofa et al., 2022; Mann, 1945).

We used the Mann–Kendall (MK) method to identify the trend in temperature and Rainfall for both historical and future periods; the historical was from 1990 to 2020, and the future was split into the midterm future (2040 to 2070) and distant future (2071 to 2100) in SSP4.5 and SSP8.5 climate scenarios.

The nonparametric method of MK has been frequently used to identify trends in hydro meteorological time series due to its dependability for recognizing monotonic patterns in climatic time series data(Bari et al., 2016; Mann, 1945). Two hypotheses have been developed: the alternative hypothesis, which has a trend in the time series, and the null hypothesis, which does not have trends. When the P-value falls below the significance level of α=0.05, the test is considered statistically significant, and the alternative hypothesis is employed, and the null hypothesis is rejected.

When the p-value exceeds the significant level (α=0.05), the null hypothesis cannot be rejected; this indicates that the test is statistically insignificant. The nonparametric method Sen's slope estimator test (Ali et al., 2019; Sen, 1968) was used to estimate the magnitude of trends in the data time series. For both Sen’s slope and the Mann-Kendall (MK) tests, a negative score indicates a declining trend; a positive value shows an increasing trend.

To compare the results, by using ArcGIS technics, we produced the distribution maps showing the spatial distribution of mean annual maximum temperature (Tmax) and

minimum temperature (Tmin) and Rainfall in the Gobele watershed; maps were produced using distance-based interpolation method, which is also known as inverse distance weighting (De Lima et al., 2010).

3.5.5 Homogeneity Test of the Simulated Data

The main extreme events in climate change analysis are temperature and Rainfall; their trend analysis was analyzed in order to know how they are enhancing the climate change in the watershed. Considering the multi-model ensemble of daily data (Rainfall, Tmax, and Tmin) for all six stations, we created the annual time series to use for the homogeneity test. Pettitt's test (Pettitt, 1979) was used to determine the most likely time for a change point in an annual time series to occur under the alternative hypothesis that the data are inhomogeneous and the null hypothesis that the data are homogeneous; the homogeneity was examined at a 5% significance level.

Given that different change points are within the same time series, data can be identified using Pettitt's method. Based on the several studies done on homogeneity testing (Che Ros et al., 2016; Getahun et al., 2021). At the 5% significance level, the data are deemed homogeneous if the test results are in opposition to the null hypothesis. When the test procedures reject the null hypothesis at a significance level of 5%, the data are considered heterogeneous.

3.6 Hydrological modeling

Soil and Water Assessment Tool was chosen to be used for this study because it is widely recognized as an effective tool for water resource management in assessing the climate and land use/cover change impacts on water resources at the river basin level (Reshmidevi et al., 2018). SWAT is readily applicable through the development of information systems. The 'GIS' interface is based on interface and is attributed to reality. The fact that this tool is freely available and easilylinked to sensitivity, calibration and uncertainty analysis tools makes it a very popular model forevaluating land use, land cover and climate change impacts (Kiros et al., 2015). Therefore, it will be used to analyze the impact of land use, land cover, and climate change on surface water balance components in the Gobele watershed in the Wabe Shebele River Basin.

SWAT works on the principle of sharing a basin into numerous sub-basins, which are

further divided into many hydrologic response units (HRUs), which are made up of uniform landcover, soil type, and topographical factors. Each HRU is used to represent the entire water balance, which includes evapotranspiration, lateral subsurface flow from the soil profile, distribution of rain, snowmelt water, redistribution of groundwater and return flow from shallowaquifers (Chaemiso et al., 2016).

The SWAT simulation of the hydrological cycle is based on this water balance equation:

$$SW_t = SW_0 + \sum_{i=1}^{t}\left(R_{day} - Q_{surf} - E_a - W_{seep} - Q_{gw}\right) \quad (3.11)$$

Where SWt is the final moisture content of the soil (mm), SWo is the initial water content of the soilon day I (mm), t is time in days, Rday is the Rainfall on day I (mm), Qsurf is the quantity of surface runoff on day I (mm), Ea is the quantity of evaporation on day I (mm), Wseep is the quantity of water entering the vadose zone from the soil profile on day i (mm). Qgw is the amount of reflux on the day I (mm). In addition, the SWAT model determined the water yield, which is a crucial factor in the sustainable management of water resources in the study area.

The total volume of water that has been thrown from the HRU and into the main channel over time is known as the water yield (Arnold et al., 2012). SWAT estimates water balance components based on the below formula:

$$W_{yld} = Q_{surf} + Q_{gw} + Q_{lat} - L \quad (3.12)$$

Where, W_{yld} is the water yield (mm), Q_{gw} is the surface runoff (mm), Q_{lat} is the lateral flow (mm), and L is the transmission loss (mm) from the tributary HRU.

The stream flow is calculated from the model simulation at the basin level by means of soil conservation service (SCS) curve number (CN); the SCS curve number method developed by the Soil Conservation Service was used to estimate stream flow from Precipitation by using the following equation:

$$Q_{surf} = \frac{(P - 0.2S)^2}{(P - 0.8S)} \quad (3.13)$$

Where S is the drainage volume of the soil water per unit area of a saturated thickness

(mm/day)

$$S = \left(\frac{25400}{CN} - 254\right) \quad (3.14)$$

3.6.1 SWAT model setup

Spatial and temporal data were used for the SWAT model setup. The spatial data includes the Model of Digital Elevation (DEM) and soil and land cover data, while the temporal data needed in the modelling process is weather data. The Digital Elevation Model is essential inthe SWAT model setup and was used for catchment delineation.

Digital Elevation Model of 30 m * 30 m resolution was obtained from the Shuttle Radar Topographic Mission (SRTM). Moreover, DEM data was used to generate slopes, which were used to define hydrological response units (HRU) together with soil and land use data.

To develop the SWAT model and the data, the Arc SWAT 2012 tool was embedded in the ArcGIS 10.5 environment. In the Gobele watershed, 71 sub-watersheds were delineated from its 1627 km^2 drainage area using DEM and stream network data. By superimposing maps of soil, land use, and slope, the 583 HRUs were defined. The slope classes used in this study were 0-5.49%, 5.49-10.99%, 10.99-18.8%, 18.88- 29.5%, and over 29.5% as the SWAT model produced. The water balance components were generated by the SWAT model using weather data subsequent to the HRU identification.

Data from 1990 to 2020, including the warm-up period of three years, were used to initialize the SWAT model. Stream flow data from 2007 to 2016 were then used to calibrate and validate the model. The implications of climate change in the study basin were then examined by evaluating the water balance components produced by the SWAT model. The soil data was found from the Food and Agriculture Organization harmonized sail database.

The prepared land use/land cover data for the years 2020, 2040 and 2070 were used for SWAT simulation in three different scenarios: scenario one was 1990-2020 (2020 LULC), scenario two was 2040-2070 (2040 LULC) and scenario three was 2071-2100 (2070 LULC).

3.6.2 Sensitivity and Uncertainty Analysis

Sensitivity analysis is the process of estimating the most sensitive parameters for a certain basin andsub-basin; it is the first stage in the calibration and validation process in SWAT. A variety of hydrological parameters related to stream flow, evapotranspiration, and water yield were selected for sensitivity analysis in the study area. The sensitivity of each parameter was identified using the T statistics and P values via the SWAT-CUP tool using the Sequential Uncertainty fitting version 2 (SUFI-2).

To conduct a stream flow sensitivity analysis, average monthly stream flow data from the Gobele watershed at Erer hydrological station were gathered for 17 years, from 2000 to 2016. The SUFI-2 approach was incorporated into SWAT-CUP 2012 version 5.1.6 due to its excellent performance in multiple Ethiopian basins (Arnold et al., 2012; Fita & Abate, 2022). Thirty hydrological parameters with default minimum and maximum bound were selected for global sensitivity analysis of SWAT-CUP and other literature(Arnold et al., 2012).

After performing thousands of simulations, the sensitivity parameters were found using multiple regression techniques utilizing Latin hypercube parameters of the target function, t-statistics, and p-values. P value was used to determine the significance of the sensitivity, and T statistics shows a measure of sensitivity; a value close to zero has more significance. T stat provides a measure of sensitivity, and the most sensitive parameters usually appear with P values less than the alpha level of 0.05(Arnold et al., 2012). The parameter values range was adjusted accordingly to get the desired values. Better parameterization gives the model the ability to be without Uncertainty.

3.6.3. SWAT model Calibration and Validation

The SWAT model was calibrated and validated against observed discharge data from the Erer hydrological station from 2000 to 2016 utilizing the SUFI-2 method of SWAT-CUP. The SUFI-2 algorithm was applied because it is frequently used in research for the SWAT model calibration on a large scale.

Its easy application and the reduced number of model runs needed to achieve a decent prediction. The mean and standard deviation of the monthly stream flow data were used to divide the calibration and validation periods. For the hydrological conditions (rain and dry years) to be distributed equally throughout both periods, there needs to be a roughly equal

mean and variance between the calibration and validation periods (Abbaspour et al., 2015).

The model was calibrated using data from 2000 to 2010 and validated using data from 2011 to 2016. The quality of the measured stream flow data from the Gobele watershed at Erer hydrological station. Several iterations were performed with hundreds of simulations for each run until reasonable minimal variations between observed and simulated stream low were found. Subsequently, the SWAT model was calibrated with parameters that showed high sensitivity.

3.6.4. Model Performance Evaluation

Testing of model performance was done to ensure that it is reliable for simulating hydrological processes. Model performance was tested using NSE, R^2 and PBIAS. The levelof similarity between simulated and observed data is indicated by Nash and Sutcliffe simulationefficiency (NSE), which is determined utilizing the subsequent formula:

$$NSE = 1 - \frac{\sum (Q_{obs} - Q_{sim})^2}{\sum (Q_{obs} - \overline{Q_{obs}})^2} \quad (3.14)$$

Where N is the number of compared values, Qobs is the observed data, $Qobs$ is the observed mean,and Qsim is the simulated data. Nash and Sutcliffe simulation efficiency (NSE) indicates Nash and Sutcliffe simulation efficiency (NSE) measures how fit the simulated and observed data are. The coefficient of determination (R^2) measures the capacity of a model in the context of linear regression to forecast or explain a result. R^2 ranges from 0 to 1, with higher values indicating less error variance, and typically values greater than 0.5 are considered acceptable (Arnold et al., 2012). The coefficient of determination is calculated by the equation below:

$$R^2 = \frac{\left[\sum \left(Q_{obs} - \overline{Q_{obs}}\right)\left(Q_{sim} - \overline{Q_{sim}}\right)\right]^2}{\sqrt{(Q_{obs} - \overline{Q_{obs}})^2 \sum \left(Q_{sim} - \overline{Q_{sim}}\right)^2}} \quad (3.15)$$

Where Qobs is the measured value, $Qobs$ is the average measured value, Qsim is the simulated value, and $Qsim$ is the mean simulated value. The following equation is used to determine per cent bias (PBIAS), which represents the mean variation between the

simulated and measured values for aparticular quantity over a specific time (often the full calibration or validation period).

$$PBIAS = \frac{(Q_{sim} - Q_{obs})}{Q_{obs}} \text{ x } 100 \qquad (3.16)$$

Where Qobs is the measured value, and Qsim is the simulated value.

The methodological framework of the study is shown in the figure below:

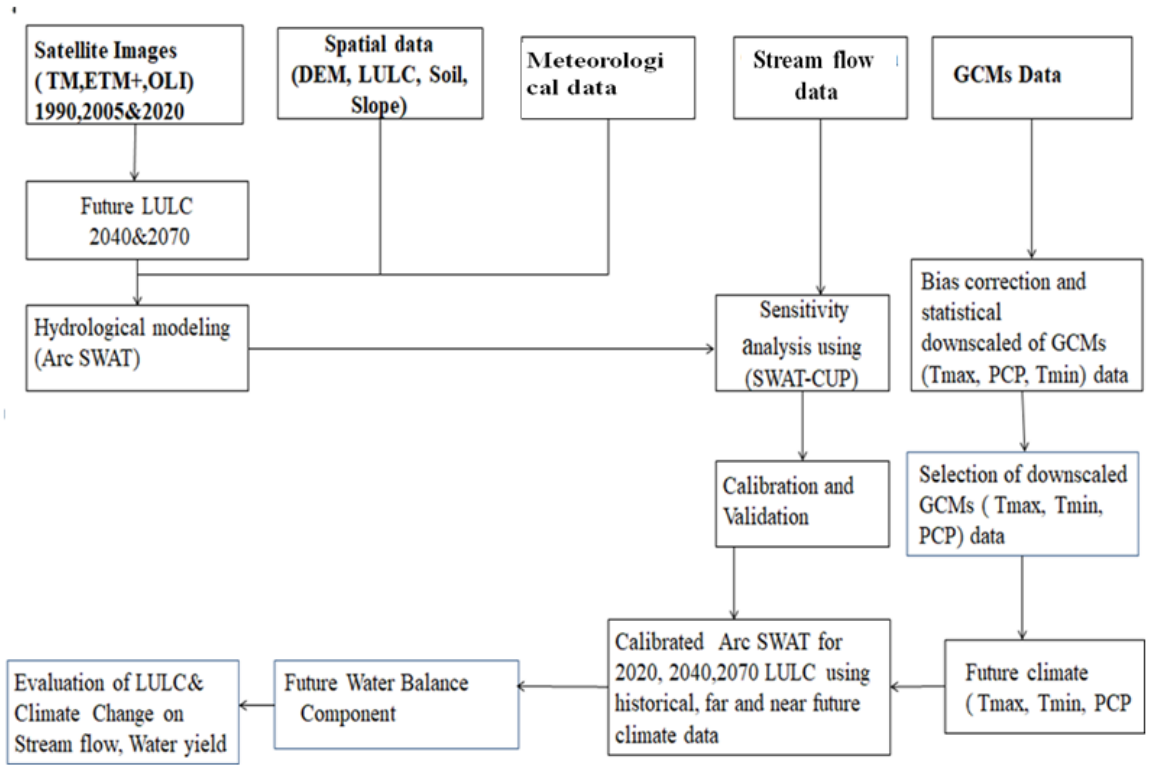

Figure3.6 Methodology flow chart for the study

4. RESULTS AND DISCUSSION

4.1 Land Use Land Cover

4.1.1 Historical Land Use Land Cover

The spatial coverage with their percentages of the six land use land cover types between 1990-2005, 2005-2020, are shown in figure 4.1 (table 4.1). The results show that for 1990-2005, grass/shrub land covers 57.10%, followed by agriculture 47.2% and barren land. Settlement is 7.5% and 7.25%, respectively.

Between 2005 and 2020, the distribution of agricultural land demonstrated the highest coverage in the watershed, which increased from 47.2% to 50.77%, followed by grass/shrub land and barren land, which was 21.63%, and 13.83%, respectively settlement was 8.91% followed by water body and forest which was 2.77% and 2.09% respectively. Grass/Shrub land and forest decreased between 1990 and 2020 by -35.46% and -1.97% respectively (table 4.1). The area of the grass/shrub land decreased due to a change of land use (conversion) to the expansion of agricultural land in the watershed. The settlement area gradually expanded from 7.25% to 8.91% over the entire historical period.

These results indicate that the land use land cover change is increasing and more likely to affect water balance components. The analysis shows that during the past 31 years, there has been an increase in agricultural, barren land, settlements, and water bodies, while there has been a significant loss in forests and grasslands in the study area. Over the study period, there was a 3.56% growth in agricultural land. This is because, as the population grows, there is a greater need for land for the production of various agricultural goods, such as industrial, field, and cereal crops, while the amount of forest area is decreasing; this may be the result of deforestation efforts made in support of urbanization and agriculture.

As a result, policies encouraging agricultural investment promoted additional deforestation, which results in land conversion (Shukla & Gedam, 2019), and different kinds of grass/shrub lands and natural forests are being demolished and replaced by commercial agriculture in different parts of Ethiopia (Stebek, 2011).

Table 4.1 Magnitude of the historical LULC types for 1990, 2005 and 2020 in the study area.

	Spatial Coverage						**Change between years**	
	1990		2005		2020		2020-1990	
LULC Classes	Sqkm	%	sqkm	%	sqkm	%	Sqkm	%
settlements	118	7.25	125	7.683	145	8.91	27	1.66
Water body	19	1.17	45	2.766	45	2.77	26	1.6
Forests	66	4.06	40	2.459	34	2.09	-32	-1.97
Agriculture	768	47.2	802	49.293	826	50.77	58	3.56
Barren land	182	7.5	146	8.974	225	13.83	43	6.33
Grass/Shrub land	869	57.1	469	28.826	352	21.63	-517	-35.5

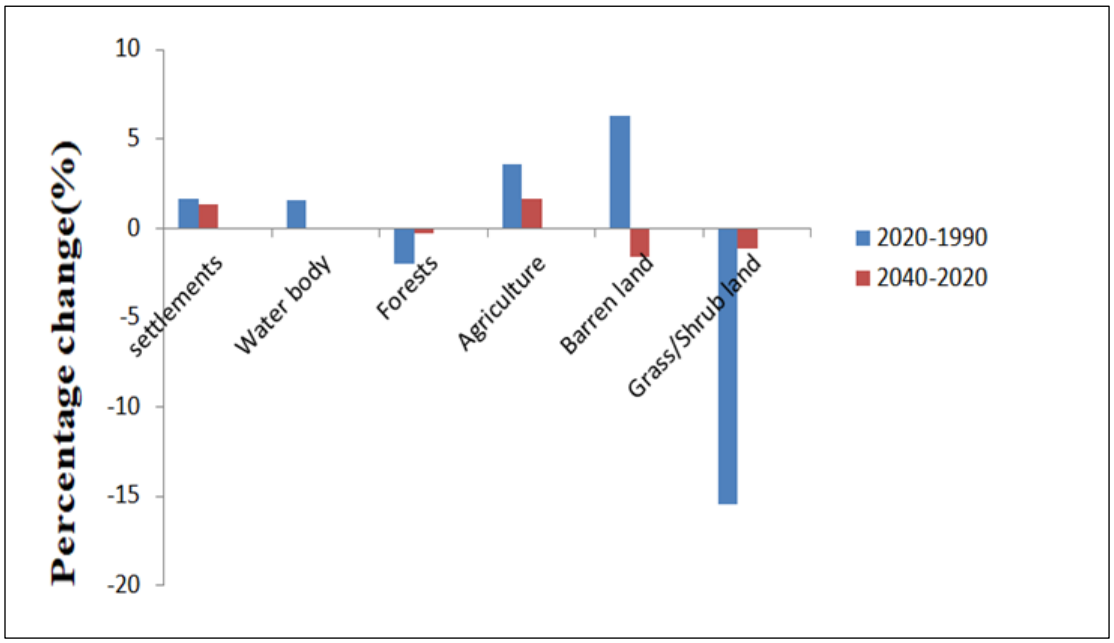

Figure4.1 Comparison of the LULC change in percentages from 1990 to 2020

Table 4.2 Confusion matrix accuracy check for the classified images

LULC Classes	1990				2005				2020			
	P.Acc	U.Acc	C.E	O.E	P.Acc	U.Acc	C. E	O.E	P.Acc	U.Acc	C.E	O.E
Agriculture(AGRL)	0.99	0.98	0.03	0.07	0.88	0.92	0.16	0.11	0.86	0.79	0.1	0.06
Forests(FRST)	1	1	0	0.01	1	0.85	0	0.01	1	0.9	0.13	0.07
Settlements(URBN)	0.86	0.79	0.04	0.07	0.87	0.87	0.17	0.13	0.89	1	0.11	0.02
Grass/Shrub land(RNGB)	0.94	0.92	0.03	0.02	0.95	0.87	0.15	0.09	1	0.96	0.08	0.14
Barren land(BARR)	0.87	0.88	0.02	0.02	0.93	0.92	0.11	0.13	0.98	1	0.14	0.12
water body(WTR)	0.91	0.84	0.03	0.1	0.87	0.95	0.05	0.14	0.97	0.96	0.19	0.09
Overall Accuracy	90.50%				85.40%				93.50%			
Kappa Coefficient	0.902				0.859				0.904			

Where P.Acc is producer accuracy, U.Acc is user accuracy, C.E is commission error, and O.E is omission error.

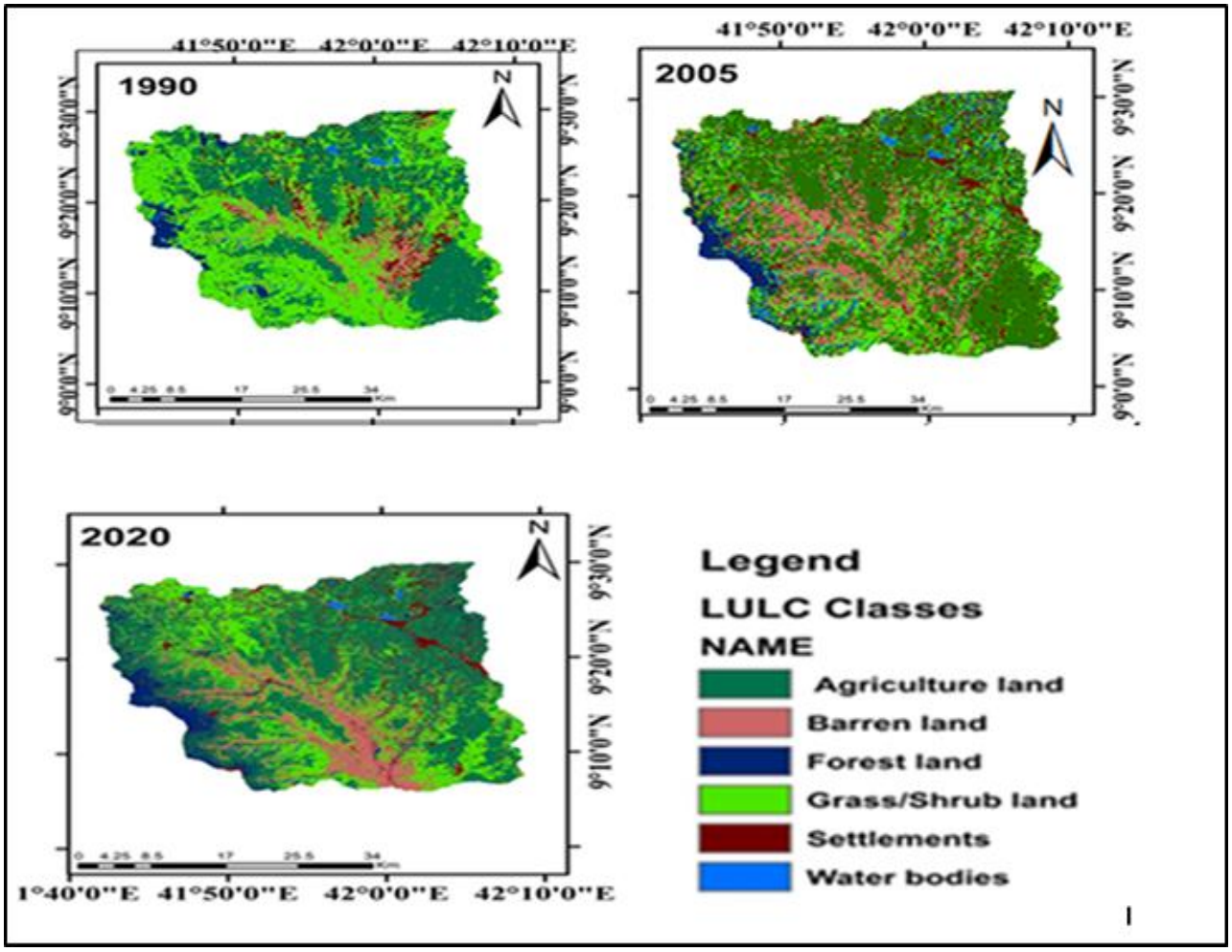

Figure 4.2 Historical land use land cover of the Gobele watershed

4.1.2 Accuracy Assessment

In this study, the accuracy assessment was performed using the 300 ground control points collected through stratified sampling using Google Earth pro for each map. Therefore, for assessing the accuracy of the LULC map of 1990, 2005, and 2020, the ground control point was produced for every single map in making a classification confusion matrix, also known as an error matrix, which is one of the most popular ways to describe classification accuracy.

The link between known reference data (ground truth) and the related outcomes of automated categorization is compared category by category using confusion matrices. These matrices are square, and the number of rows and columns reflects the number of

categories for which the accuracy of the classification is being evaluated (Nguyen, 2015). The overall accuracies obtained were 91%, 85%, and 94% for 1990, 2005, and 2020, respectively (Table 4.2). The overall accuracy was calculated by dividing the correct classification by the total number of reference pixels in the error matrix.

4.1.3. Future Land Use Land Cover Prediction

The land use maps from 1990 and 2005 were used as inputs. Here, important driving variables like elevation, distance from roads, and distance from streams were included in addition to two distinct LULC period maps. Future LULC maps of the study region for 2040 and 2070 were projected using the LULC maps from 1990 and 2005. The 2020 observed LULC maps of the Gobele watershed were used to validate the LULC change prediction. Validation of the model prediction was done to see how well the simulated and reference maps agreed.

The overall Kappa indices were calculated to show the degree of agreement between the reference and comparison maps. A Kappa index of 0.89 was obtained throughout the validation phase, indicating a strong correlation between the predicted and real maps and the validity of the model's prediction (Keshtkar & Voigt, 2016). The CA-Markov chain model was used to create simulation maps for the years 2040 and 2070 following the successful validation of the 2020 actual map. Gobele watershed LULC classes were divided into six classes: agriculture land, settlements, barren land, grass/shrub land, forests, and water bodies.

In 31years, agricultural land and settlements have increased by 1.78% and 1.23%, respectively (Table 4.1), while forest land, grass/shrub land, and water bodies have reduced by -0.61%, -2.34% and -0.06%; barren land has shown the decreasing pattern in historical LULC, and it became constant between 2040 and 2070.

Alongside this, improper methods of conserving water and soil are being used, and the population of the watershed is growing. The main factors influencing changes in land use and land cover in the watershed area include population shifts, changes in land tenure, poverty, and a lack of access to credit and markets (Guduru & Jilo, 2022; Gurara et al., 2021; Woldemariam et al., 2018; Woldemariam & Harka, 2020).

Table 4.3 Magnitude of the projected LULC types for 2020, 2040, and 2070 in the study area.

	Spatial coverage						Change between years			
LULC Classes	2020		2040		2070		2070-2020		2070-2040	
	Sqkm	%	sqkm	%	sqkm	%	sqkm	%	sqkm	%
settlements	145	8.91	167	10.3	187	11.494	42	2.58	20	1.23
Water body	45	2.77	45	2.77	44	2.7044	-1	-0.06	-1	-0.06
Forests	34	2.09	29	1.78	19	1.1678	-15	-0.92	-10	-0.61
Agriculture	826	50.77	853	52.4	882	54.21	56	3.44	29	1.78
Barren land	225	13.83	199	12.2	199	12.231	-26	-1.6	0	0
Grass/Shrub land	352	21.63	334	20.5	296	18.193	-56	-3.44	-38	-2.34

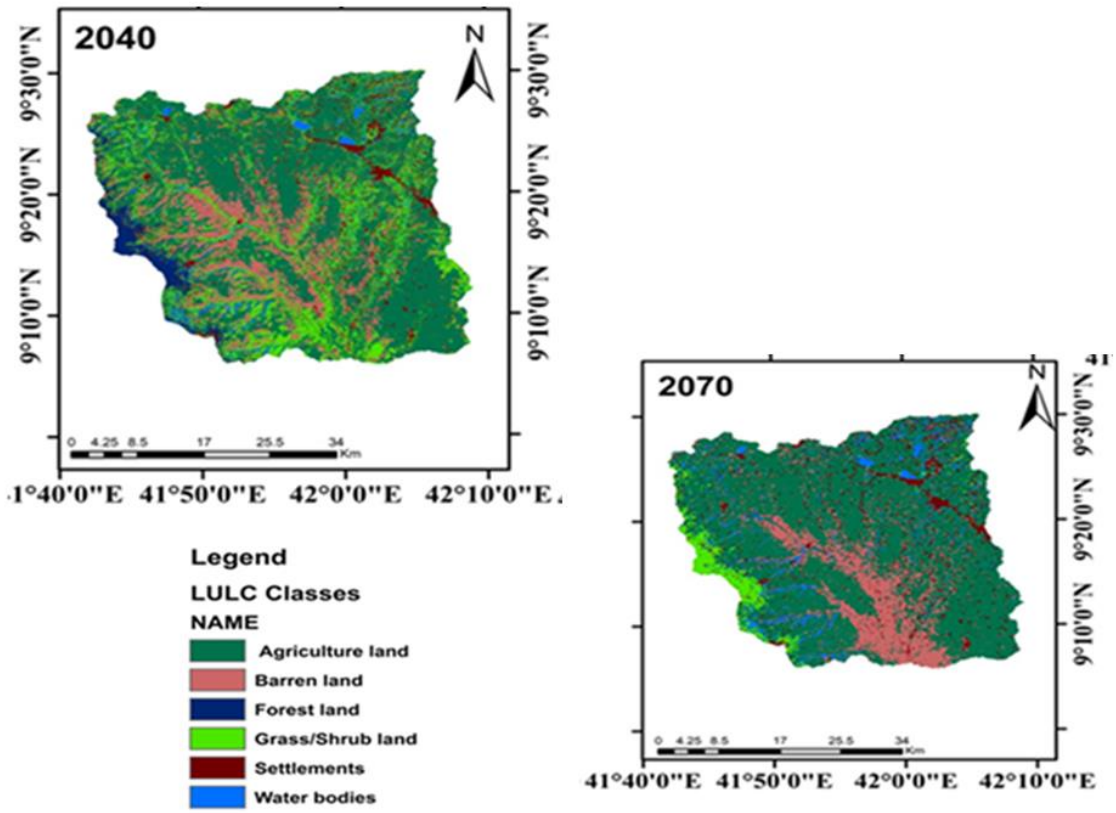

Figure 4.3 Future land use land cover of Gobele watershed.

4.2 Evaluation of Multi-Model Ensemble Climate Projection

To evaluate the performance of the multi-model ensemble for climate projection, a comparison between monthly simulated historical data and monthly observed historical data for Rainfall, Tmax, and Tmin data at all six stations was used. For observed Rainfall, the results of the multi-model ensemble show a positive correction coefficient over all stations, with R^2, RMSE, and PBIAS values ranging between 0.51 and 0.76, 0.27 and 4.5 mm, and -4.2% to 18.7%, respectively. Therefore, the multi-model ensemble mean data agreed with the observed data at all stations (Table 4.3). For both maximum and minimum temperature, R^2 values and RMSE range from 0.56 to 0.93 and 0.26 to 2.5 respectively, and PBIAS values range from -0.78% to 5.2%. This demonstrates that the multi-model ensemble performed well, with better agreement between observed and simulated Tmin and Tmax values at all stations in the Gobele watershed. Note that the historical and observed climate data were considered from 1990 to 2020.

Table4.4 Statistical performance of the multi-model ensemble of monthly Rainfall, Tmin, and Tmax from 1990 to 2020.

	Rainfall			**Maximum Temperature**			**Minimum Temperature**		
Stations	R^2	RMSE (mm)	PBIAS (%)	R2	RMSE (mm)	PBIAS (%)	R2	RMSE (mm)	PBIAS
Alemaya	0.76	0.27	-4.2	0.93	0.26	-0.78	0.89	0.31	-0.59
Daawe	0.51	4.5	18.7	0.61	2.5	2.03	0.72	1.78	1.04
Dengengo	0.67	1.79	1.42	0.77	1.11	1.23	0.64	0.56	1.73
Girawa	0.71	2.84	-0.9	0.84	2.12	-0.66	0.56	2.0	3.79
Huse	0.58	3.2	3.5	0.55	1.71	4.51	0.54	2.5	5.2
Woter	0.62	1.65	2.1	0.83	2.01	0.12	0.83	1.34	0.7

4.3 The Trend Analysis of Historical and Future Climate Parameters

The trend analysis, as well as the spatial distribution of historical and future rainfall and temperature (maximum and minimum) data, were evaluated in the Gobele watershed on both monthly and annual basis in different time intervals: historical (1990–2020) and future (2040–2070 and (2071–2100) under medium and high emission scenarios (SSP2-4.5 and SSP58.5).

4.3.1 Historical Annual Rainfall and Temperature Trends Analysis

In this study, we used the XLSTAT add-in software in an excel sheet by means of the Mann-Kendall trends test, P-value, and Sen's slope estimator's results for historical Rainfall, Tmin, and Tmax. The Mann-Kendall trends test for mean annual rainfall data was tested at the 5% significance level; the results show an insignificant increasing or decreasing trend in most of the stations under certain conditions of MK and Sen's slope, and by considering the P-value, the ensemble climate models show the increasing pattern in all the stations.

The historical data of Tmax and Tmin has shown an insignificant increasing or decreasing pattern for MK, P-value, and Sen's slope trend analysis test variables at most of the stations except for Girawa, where both minimum and maximum temperatures show a decreasing pattern, Alemaya and Daawe Tmax shown decreasing pattern and Woter where Tmin has also shown the decreasing trend. The growing trends on the simulated and actual slopes were almost the same; this proves the usefulness of using downscaled Tmax and Tmin data for trend analysis. The fact that the simulated and observed slopes showed the same rising trends further validated the value of using downscaled Tmax and Tmin data for trend analysis.

Table4.5 Mann-Kendall and Sen's Slope estimator value for annual Rainfall, Tmax, and Tmin in the study area from 1990 to 2020.

Parameters	**Rainfall**			**Tmax**			**Tmin**		
Tests → / Stations ↓	MK Test	P-value	Sen's Slope	MK Test	P-value	Sen's Slope	MK Test	P-value	Sen's Slope
Alemaya	0.12	0.36	0.01	0.38	0.00*	0.03	-0.25	0.05	-0.03
Daawen	-0.25	0.05	-0.01	0.41	0.00*	0.12	0.13	0.32	0.04
Dengego	0.09	0.46	0.01	0.24	0.06	0.04	0.03	0.84	0.00
Girawac	-0.02	0.87	0.00	-0.66	<0.00*	-0.09	-0.38	0.00*	-0.04
Huse	0.12	0.36	0.01	0.03	0.84	0.00	0.23	0.07	0.02
Woter	0.01	0.96	0.00	0.07	0.59	0.01	0.30	0.02*	0.02

* indicate the significant increase or decrease trends, whereas – decreasing trend and + increasing.

Using inverse distance weighting, the spatial distribution of the historical mean annual Rainfall and temperature maps across the Gobele watershed during the period of 1990–2020 was developed for both observed and simulated data (Figure 4.4). The results showed almost similar patterns in both mean annual observed data and historical data (Rainfall, Tmin, and Tmax). Based on the Rainfall (Figure4.4 a, d), it is clearly shown that the upper-western part of the watershed receives higher Rainfall than the rest parts of the watershed. It agrees with model outputs from simulations as well as observations. Moreover, the spatial distribution of Tmax (Figure4.4 c, f) and Tmin (Figure4.4 b, e) shows a similar distribution where it ranges between 21℃ to 31℃ and 9℃ to 17℃ respectively; the western parts of the watershed show the highest temperature and lower in the upper eastern part of the watershed.

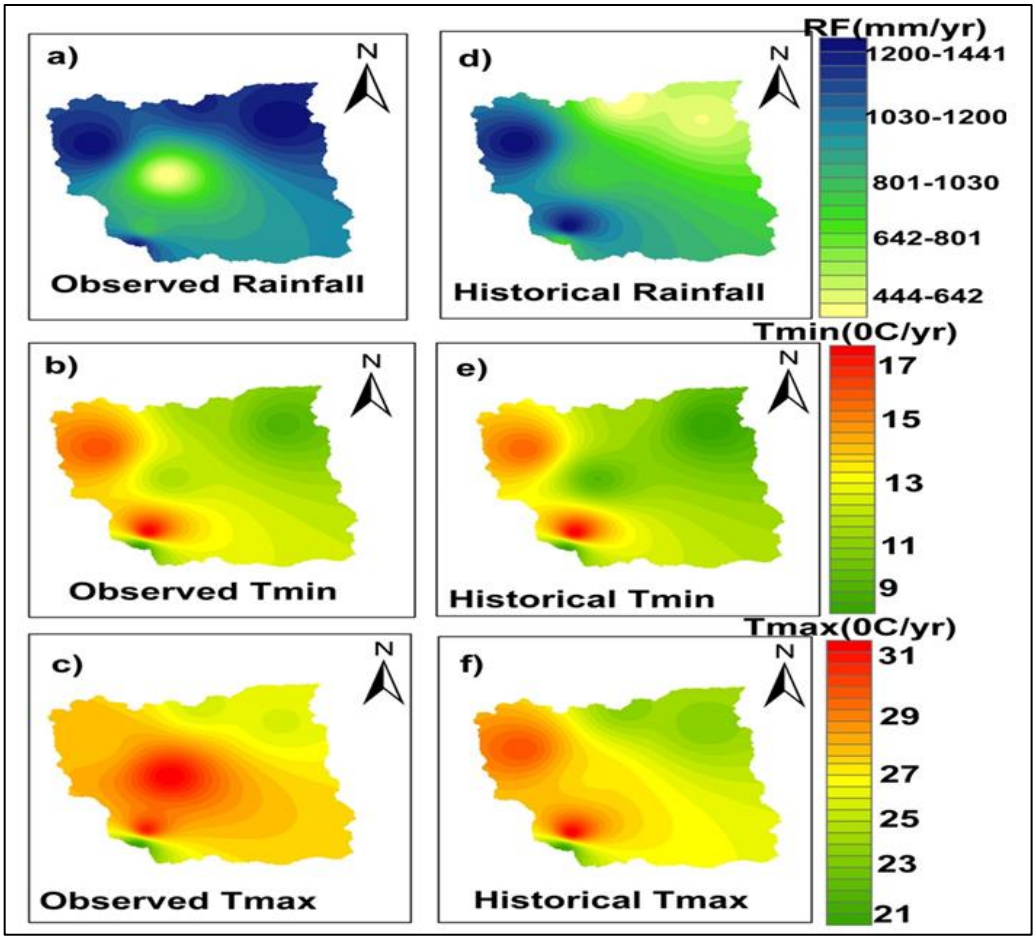

Figure4.4 Spatial distribution of the observed and multi-model ensemble of annual Rainfall (mm/yr), Tmax(℃/**yr**), and Tmin (℃/**yr**) over the Gobele watershed (1990-2020) for **a)** observed Rainfall, **b)** observed Tmin, **c)** observed Tmax, **d)** historical rainfall, **e)** historical Tmin, **f)** historical T max. All data ae after bias correction.

4.3.2 Future Annual Rainfall and Temperature Trends

To analyze the future trends, the medium (SSP2-4.5) and high (SSP5-8.5) emission scenarios were used to examine the potential trends in mean annual Rainfall, Tmax, and Tmin in the midterm future (2040-2070) and distant future (2071-2100) periods. The rainfall trend analysis for both scenarios from 2040 to 2070 is shown in Table 4.5. For the SSP2-4.5 scenario, the annual mean Rainfall increased insignificantly at all six stations at a 5% significant level. For the SSP5-8.5 scenario, four of the six stations in the study area have shown insignificant increasing patterns, and the other two (Huse and Woter) have shown significant increases at the 5% significance level. Considering Sen's slope estimator, the minor rise and fall of 0.01 and 0.02 mm/year and 0.02 and 0.04 mm/year under SSP2-4.5 and SSP5-8.5, respectively, was observed.

Table 4.6 Mann-Kendall and Sen's Slope estimator results for future annual Rainfall over the six stations in the Gobele watershed (2040-2070), (2071-2100).

	Future rain fall 4.5&8.5(2040-2070)						**Future rain fall 4.5&8.5(2071-2100)**					
Tests	SSP2-4.5			SSP5-8.5			SSP2-4.5			SSP5-8.5		
Stations	MK Test	P-value	Sen's Slope	MK Test	P-value	Sen's Slope	MK Test	P-value	Sen's Slope	MK Test	P-value	Sen's Slope
Alemaya	0.13	0.32	0.02	0.11	0.38	0.02	-0.02	0.89	0.00	0.16	0.23	0.05
Daawe	0.11	0.38	0.01	0.14	0.29	0.02	-0.05	0.69	-0.01	0.10	0.43	0.03
Dengengo	0.11	0.38	0.02	0.11	0.40	0.02	-0.06	0.64	-0.02	0.14	0.27	0.04
Girawa	0.13	0.31	0.01	0.14	0.29	0.02	0.12	0.35	0.01	0.11	0.41	0.03
Huse	0.13	0.31	0.01	0.28	0.03*	0.04	0.09	0.50	0.01	0.12	0.35	0.03
Woter	0.12	0.34	0.02	0.28	0.03*	0.04	0.01*	0.94	0.02	0.12	0.37	0.03

* indicate the significant increase or decrease trends, whereas – decreasing trend and + increasing.

The results showed an increase in Rainfall between 2071 and 2100, with values ranging from -0.02 to 0.02 mm/year and 0.03 to 0.05 mm/year under SSP2-4.5 and SSP5-8.5, respectively. In the distant future (2070–2100), the annual Rainfall shows an increasing pattern at all stations at 5% significance level under the SSP2-4.5 scenario. Similar changes were observed in the SSP5-8.5 scenario (Table 4.5). Moreover, both SSP2-4.5 and SSP5-8.5 scenarios have minor increases in the mean annual rainfall patterns of the Gobele watershed during the future periods of 2040–2070 and 2071-2100.

The midterm-future (2040–2070) Tmax and Tmin multi-model ensemble trend results for the SSP2-4.5 and SSP5-8.5 scenarios demonstrated that at the 5% level of significance, both the SSP2-4.5 and SSP5-8.5 scenarios show significant increases across all stations (Table4.5).

Under SSP2-4.5 and SSP5-8.5, the far-future (2070–2100) Tmax and Tmin showed

insignificant increases, except that some stations (Huse, Girawa, Woter) which show significant increases in the Tmin trends under midterm-future period under SSP2-4.5 scenario at 5% significance levels, and at Girawa and Woter stations shows the significant increases under SSP5-8.5 scenario. Generally, Tmax and Tmin showed significant increases at the 5% significance level in the future period (2040–2099) under SSP2-4.5 and SSP5-8.5 scenarios over the Gobele watershed.

Table 4.7 Projected Mann-Kendall and Sen'Slope statistical estimator results for annual Tmax and Tmin from six stations over the Gobele watershed (2040-2070) and (2071-2100).

	Future temperature 4.5&8.5(2040-2070)						**Future temperature 4.5&8.5(2071-2100)**					
Climate Parameter	Tmax SSP2-4.5			Tmax SSP5-8.5			TminSSP2-4.5			TminSSP5-8.5		
Tests	MK Test	P-value	Sen's Slope	MK Test	P-value	Sen's Slope	MK Test	P-value	Sen's Slope	MK Test	P-value	Sen's Slope
Stations												
Alemaya	0.46	0.01*	0.06	0.66	0.00*	0.16	0.18	0.16	0.03	0.55	0.05	0.08
Daawe	0.49	0.00*	0.06	0.59	0.00*	0.06	0.26	0.05	0.03	0.33	0.32	0.04
Dengengo	0.44	0.00*	0.04	0.74	0.00*	0.04	0.18	0.18	0.02	0.17	0.84	0.11
Girawa	0.49	0.01*	0.04	0.69	0.00*	0.14	0.26	0.04*	0.03	0.38	0.00*	0.08
Huse	0.50	0.00*	0.03	0.70	0.00*	0.03	0.28	0.03*	0.02	0.23	0.07	0.07
Woter	0.49	0.02*	0.03	0.79	0.00*	0.10	0.29	0.03*	0.02	0.30	0.02*	0.18

* indicate the significant increase or decrease trends, – decreasing trend and + increasing.

Through the use of inverse distance weighting of the multi-model ensemble data under SSP2-4.5 and SSP5-8.5 scenarios, the spatial distribution of projected mean annual Rainfall within the Gobele watershed was investigated (Figure 4.4). The findings indicate that there is a chance that the mean annual rainfall distribution in the future will have the same changing pattern as the historical distribution from 1990 to 2020 in terms of spatial distribution (Figure 4.4). Future rainfall values in the upper part of the Gobele watershed

are anticipated to rise marginally. Moreover, the difference in elevation and land use land cover within the watershed can cause an unequal distribution of the rainfall pattern.

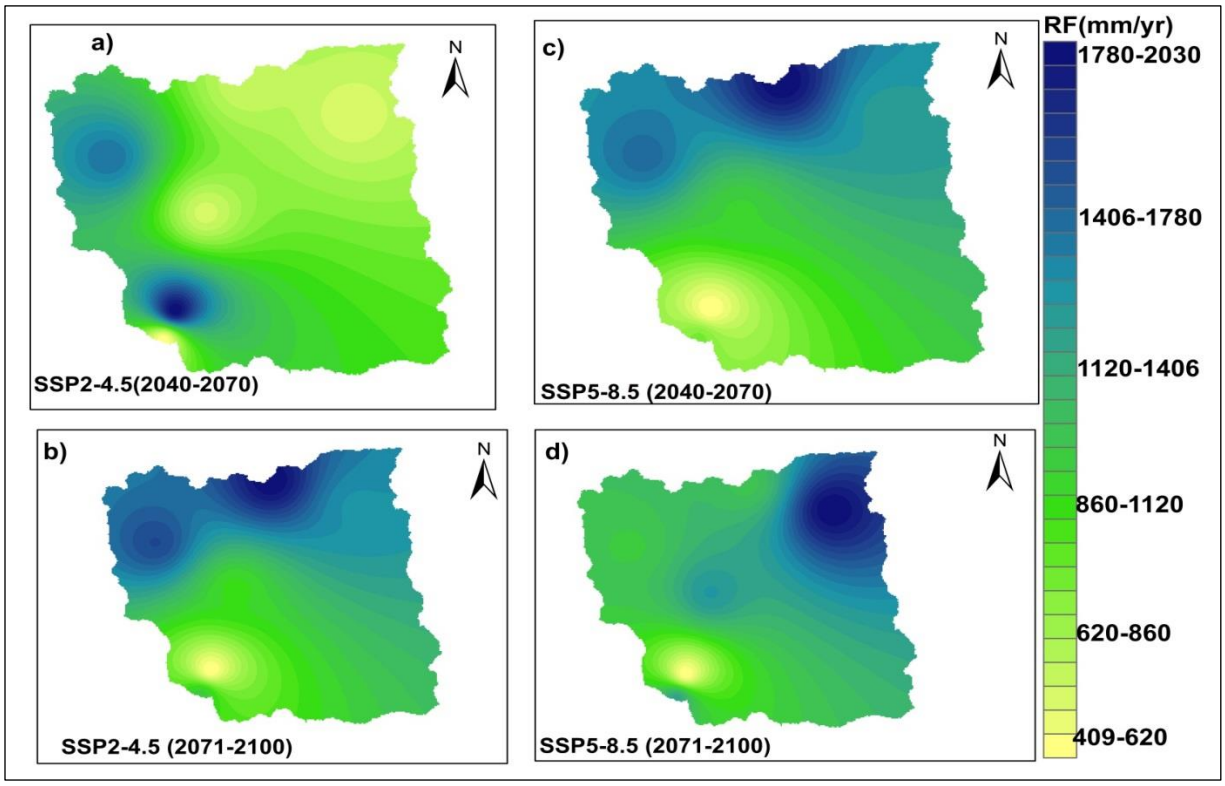

Figure4.5 Spatial distribution of the multi-model ensemble of mean annual Rainfall in the Gobele watershed over two future scenarios (SSP2-4.5 and SSP5-8.5) **a)** midterm future SSP2-4.5, **b)** distant future SSP2-4.5, **c)** midterm future SSP5-8.5, **d)** distant future SSP5-8.5

In addition, the spatial distribution of Tmax and Tmin, the multi-model ensemble under both SSP2-4.5 and SSP5-8.5 scenarios, were obtained by using the inverse distribution weighting method with the help of Arc GIS software (Figure4.6 and Appendix 1). The historical spatial distribution and the anticipated Tmax and Tmin are likely to have a similar distribution. In Comparison to historical values, the projected Tmax and Tmin values under various scenarios demonstrate an increasing pattern over the Gobele watershed. Tmin is expected to range from 13°C to 23°C, while Tmax is predicted to be between 23°C and 34°C.

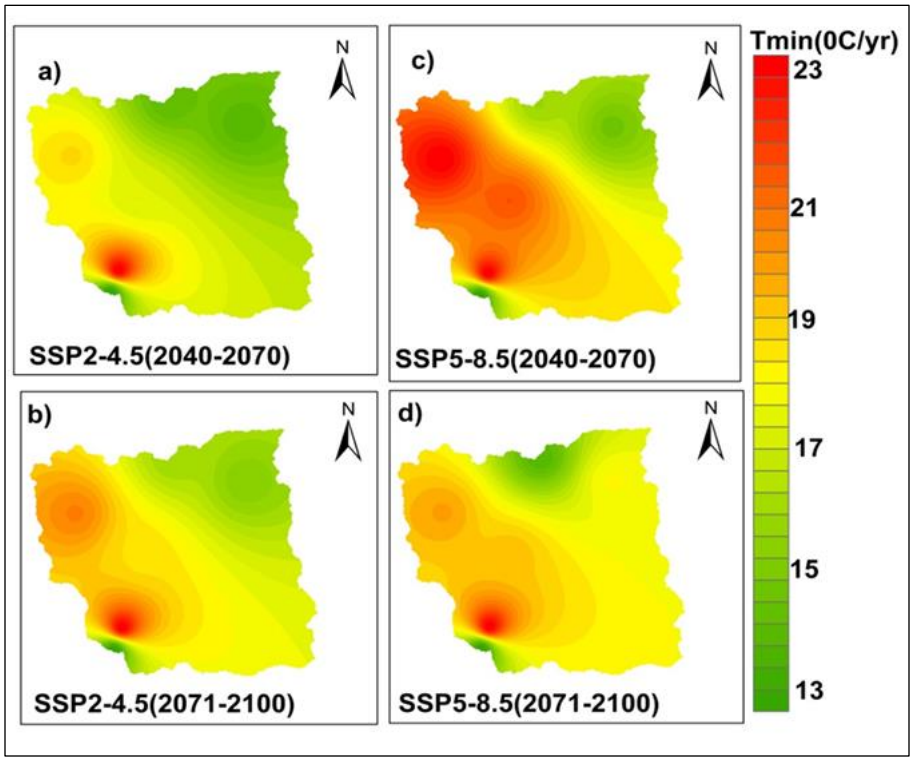

Figure4.6 Spatial distribution of the multi-model ensemble annual Tmin over Gobele watershed in two future periods and climate scenarios **a)** midterm future SSP2-4.5, **b)** for future SSP2-4.5, **c)** midterm future SSP5-8.5, **d)** distant future SSP5-8.5

4.4. Homogeneity Analysis of Future Climate Parameters

The Buishand's range test and Pettitt's test were used in homogeneity testing of the annual Rainfall, Tmax, and Tmin at all the stations under SSP2-4.5 and SSP5-8.5 scenarios for both midterm future (2040-2070) and far future (2071-2100) periods.

The results revealed that rainfall and temperature data between 2040 and 2070 were homogeneous except at Huse station, and for 2071 and 2100, all climate parameters have shown homogeneity except for some minor changes. The annual rainfall series change point was determined at 2078 for all stations (except Daawe and Woter) by Pettitt's test and Buishand's range test, whereas the change point for Tmax and Tmin was found at 2073 and 2083 for all stations, respectively.

For other stations, Buishand's range test and Pettitt's test did not indicate any break in annual Rainfall, Tmax, and Tmin under SSP2-4.5 and SSP5-8.5 emission scenarios.

4.5. SWAT Model Evaluation

4.5.1 SWAT Model Sensitivity Analysis, Calibration, and Validation

Sensitivity analysis is employed in the SWAT model to determine the critical parameters influencing stream flow (Kiros et al., 2015). Both P-value and t-stat are used for the sensitivity analysis of the hydrological model; the p-value indicates the significance of the sensitivity, and the t-stat is the parameter coefficient divided by its standard error. The calibration and validation phases involved the use of monthly stream flow data from 2000 to 2011 and 2012 to 2016, respectively. For global sensitivity analysis, 25 SWAT parameters were adopted, and 14 of them demonstrated flow sensitivity based on their t-statistic and p-value. The top six sensitive parameters were V__GWQMN.gw, A__EPCO.bsn, V__CH_N1.sub, R__HRU_SLP.hu, R__GW_REVAP.gw, and R__CN2.mgt (Table 4.8).

To ensure the improved model performance during calibration, selected parameters were repeatedly varied in an acceptable range until a reasonable match was found between observed and simulated inflow for all the land use land cover and weather data used for the SWAT model set-up (Table4.9).

Table 4.8 Sensitive flow SWAT parameters of the study area

Parameters	Description	t-Stat	p-Value	Rank
V__GWQMN.gw	The threshold depth of water in the shallow aquifer is required for return flow to occur (mm).	31.253	0.000	1
A__EPCO.bsn	Plant compensation factor at the main channel	26.213	0.000	2
R__HRU_SLP.hru	Average slope steepness	9.835	0.000	3
V__CH_N1.sub	Main channel Manning's coefficient	7.994	0.000	4
R__GW_REVAP.gw	Groundwater “revap” coefficient	6.321	0.000	5
R__CN2.mgt	SCS runoff curve number	6.230	0.000	6
R__CH_K2.rte	Effective hydraulic conductivity in main channel alluvium	6.060	0.000	7
R__REVAPMN.gw	Threshold water in the shallow aquifer for revamp to occur (mm)	5.364	0.000	8
R__SOL_AWC (..).sol	Available water capacity of the soil layer	4.324	0.000	9
V__GW_DELAY.gw	Groundwater delay time	-4.276	0.000	10
R__CH_W1.sub	Average width of tributary channels (m)	4.273	0.000	11
R__RCHRG_DP.gw	Deep aquifer percolation fraction	4.260	0.000	12
V__ALPHA_BF.gw	Base flow alpha factor (days)	3.554	0.001	13
R__OV_N.hru	Manning's "n" value for overland flow	1.724	0.03	14

Where V_Replace: replaces the parameter's current value with a specified value, R_Relative: updates the parameter's value by multiplying the fixed values (in each HRU) by the same coefficient, and A_Absolute: adds the given value to the existing value.

Table 4.9 Calibrated parameters with their fitted values

Parameters	Minimum	Maximum	Fitted Value		
			1990-2020(S1)	2040-2070(S2)	2071-2100(S3)
V__GWQMN.gw	1485.414	1801.373	1682.967	1322.902	1287.853
A__EPCO.bsn	0.800	1.000	0.900	0.731	0.872
R__HRU_SLP.hru	0.15	0.31	0.1707	0.192	0.231
V__CH_N1.sub	0.080	0.180	0.1212	0.102	0.117
R__GW_REVAP.gw	0.090	0.234	0.199	0.201	0.213
R__CN2.mgt	-0.200	0.200	-0.1917	0.131	0.168
R__CH_K2.rte	54.592	163.908	76.154	62.786	129.231
R__REVAPMN.gw	153.639	461.359	425.587	392.917	279.021
R__SOL_AWC (..).sol	0.484	1.453	1.179	1.273	0.982
V__GW_DELAY.gw	0.000	500.0	316.375	263.645	196.832
R__CH_W1.sub	-0.033	-0.230	-0.030	-0.021	-0.012
R__RCHRG_DP.gw	0.000	1.000	0.557	0.481	0.329
V__ALPHA_BF.gw	0.000	1.000	0.812	0.761	0.671
R__OV_N.hru	0.050	24.000	20.713	18.420	14.029

4.5.2 SWAT Model Performance Evaluation

The performance of the SWAT model was evaluated by comparing the observed and simulated monthly mean stream flow at the out let of the Erer station of the Gobele watershed, which was used in both calibration and validation in three scenarios (Table4.9). R^2, NSE, and PBIAS were used to assess the hydrological model's overall performance, and they have shown positive performance. According to Moriasi et al. (2015), R^2, NSE, and PBIAS greater than 0.6, 0.5, and less than or equal to zero, respectively, meet the performance criteria for estimating flow in the SWAT model at the watershed level and can be considered adequate.

After comparing the simulated and observed river discharges at the three chosen scenarios (Figure 4.7), the parameters listed in Table 4.8 were calibrated and validated. Compared to the performance evaluation parameters in all scenarios, S3 was the best over the others in the watershed; the validation and calibration cycle of S1 and S2 showed reasonable performance (Figure 4.7). The PBIAS negative value indicates the over

simulation between simulated values and observed values for both the validation and calibration periods of the three scenarios. During calibration and validation, the statistical indicators produced flawless outcomes. Throughout the calibration period, R2, NSE, and PBIAS values were 0.86, 0.76, and 14.5%, respectively; during the validation period, R2, NSE, and PBIAS values were 0.91, 0.69, and -17.4%, respectively.

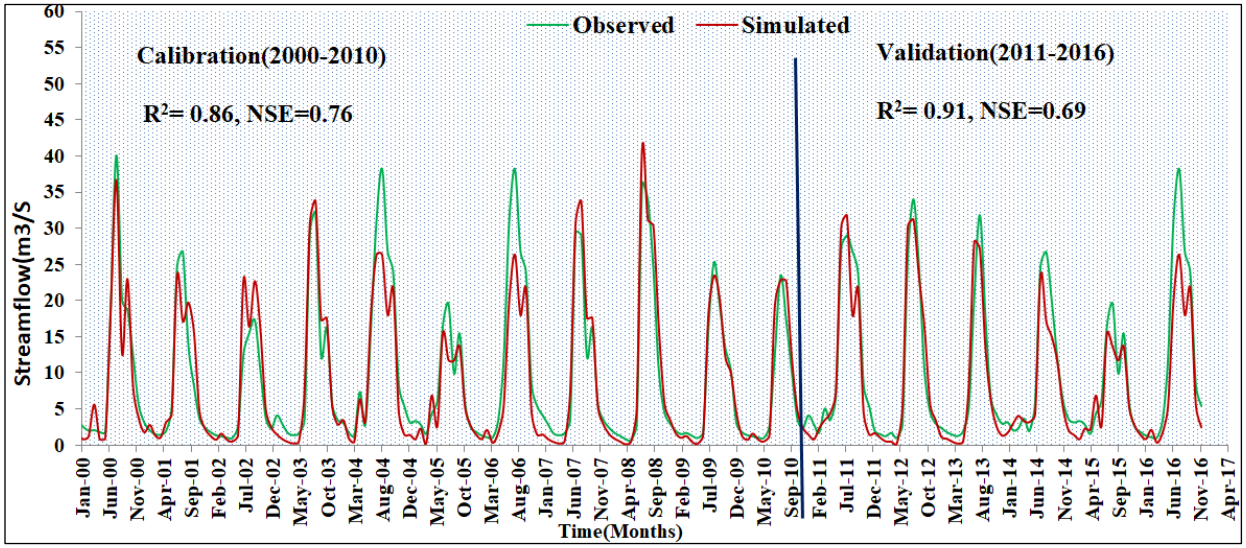

Figure 4.7 Calibration and Validation of stream flow data

4.6 Impact Evaluations Framework

The water balance component response of the Gobele watershed to the effects of LULC and climate change was studied for two future periods (2040–2070) and (2071-2100). The years 1990 through 2020 comprise the baseline era. Trios of simulation scenarios were developed to examine the individual and combined effects of land-use change and climate change. As a result, only LULC is considered in the first scenario (S1), only climate change is considered in the second scenario (S2), and both LULC and climate change are considered in the third scenario (S3). The scenario description is shown in the Table4.9.

Table 4.10 Scenarios considered during the evaluation of the impact of climate and LULC change on water balance components.

Scenarios	Description
S1	Only LULC change: land use maps of 2020, 2040, and 2070 with baseline climate data from 1990 to 2020 were used.
S2	The only map used was the 2020 baseline land use map for climate change, with three
Q	different climate scenarios: 1990–2020, 2040–2070, and 2070–2100.
S3	Land use maps of 2020, 2040, and 2070 were utilized with 1990–2020, 2040–2070, and 2071–2100 climatic data, respectively, to combine LULC and climate change.

4.6.1 LULC Change Impacts on Gobele Water Balance Components

This section examined the effects of LULC changes on water balance components on a seasonal basis. Assuming that there was no change in the climate, the calibrated SWAT model was run under two LULC change scenarios (2040–2070) and (2071–2100). Therefore, in this scenario, the effects of LULC change on stream flow, evapotranspiration, and water yield were taken into account. The analysis was based on the three climate seasons that are commonly known in Ethiopia, which are the long rain season (from June to September), the dry season (from October to February), and the short rain season (from March to May). During the short rain season (March to May) and dry season (October to February), stream flow showed a decrement of 9.76% and 24.42%, respectively.

In contrast, the increasing pattern of 31.07% during the long rain season (June to September) was observed by (2040-2070). Also, during the (2071-2100) period, stream flow has shown decrement in the dry season (October to February) by 26.57% and increased during long rain and short rain by 31.39% and 2.68%, respectively.

In the anticipated LULC transition, stream flow has generally increased compared to the baseline; nevertheless, the pace of change is small in Comparison to the individual effects of climate change. In the midterm future period (2040-2070), water yield will decrease by 10.49% and 2.46% in the dry season and short rain seasons, respectively, and will

increase in the long rainy season. In the far-future period (2071-2100), water yield will increase by 13.58% during the long rainy season and decrease by 2.19% and 10.97% during the short rain season and the dry seasons, respectively.

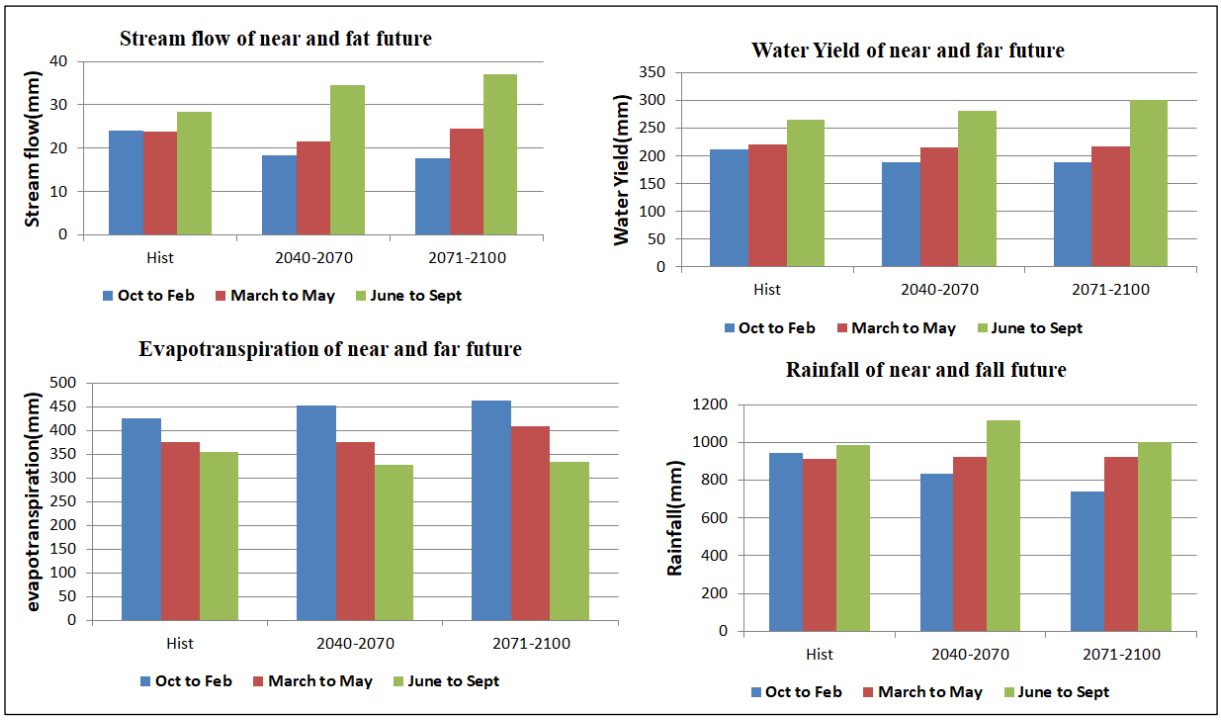

Figure4.8 Projection of mean seasonal impacts of LULC change on Gobele water balance components

The seasonal change of evapotranspiration in the Gobele watershed increased under the midterm future LULC (2040-2070) in the dry season by 5.89%, and it decreased in short rain and long rain season by 5.51% and 7.83%. In the distant future LULC (2071-2100), evapotranspiration increased in the dry season and short rain by 8.47% and 2.89%, respectively, and declined during the long rain season by 5.98%. These water balance component changes were observed due to the increases in both agricultural land and settlements, which encourages the increases in stream flow; the decrease in forestland has encouraged the decreases in evapotranspiration and increases the water yield.

4.6.2. Climate Change Impacts on Gobele Water Balance Components

As previously indicated, two climate predictions, namely SSP2-4.5 and SSP5-8.5, were taken into account in the study since it was thought that these scenarios may depict both the best and worst possible future climate conditions. From a workable multi-model ensemble of four GCMs from CMIP6, the most significant climate variables affecting stream flow generation, such as temperature and precipitation, were extracted for six selected meteorological stations.

The impacts of scenario two (S2) of climate change alone on stream flow, evapotranspiration, and water yield are examined in this section. SWAT modeling of the projected stream flow based on the three scenarios, i.e., three-time slices (1990–2020) baseline, (2040–2070) midterm future, and (2071–2100) distant future are presented from SSP2-4.5, and SSP5-8.5 predicted temperature and precipitation (Table 4.7).

To ascertain the effects of climate change on water balance components, the calibrated SWAT model was simulated in two climate change scenarios under SSP2-4.5 and SSP5-8.5, presuming that the 2020 LULC map remained constant. For possible climate change (Table 4.11) displays the mean seasonal change in evapotranspiration. The most intriguing result of this scenario was that evapotranspiration is predicted to rise by around 9.54% and 10.07% in the (2040-2070) under SSP2-4.5 and SSP5-8.5, respectively, in the dry season.

Also, it will rise by 1.53% and 0.82% under the same scenario in the short rainy season. From 2071 to 2100, in dry and short rain seasons, evapotranspiration has shown an increasing pattern by 20.72%, 20.24%, and 8.55%, 8.23% under SSP2-4.5, SSP5-8.5 scenarios, respectively, in the long rain season (June to September) evapotranspiration has shown the declining pattern under all the scenarios and periods, the decreases rate ranges of 18.94% under SSP5-8.5 scenario and 2.25% under SSP2-4.5 scenario.

In the three seasons, water yield shows the alternative increases and decreases pattern; in short rain and long rain seasons, it will increase in all scenarios in the range of 0.82% to 10.66%, whereas dry season water yield will decrease in the range of 4.5% to 6.19%. However, sudden increases were observed in the SSP5-8.5 by 10.51% from 2040 to 2070 (Table 4.11).

Moreover, the degree of water yield modification under SSP5-8.5 is observed to be higher compared to the Water yield in the SSP2-4.5 prediction scenario. The mean seasonal stream flow has shown the same changing pattern with the water yield; stream flow is likely to decrease during short rainy and dry seasons by the range of 9.13% to 14.8% respectively in both scenarios, but likely increased in long rainy seasons under the SSP2-4.5 scenario by a range of 3.56% to 22.16% in midterm future (2040-2070) while showing a decreasing pattern in all seasons under the same scenario in the distant future by 13.2%, 9.82% and 16.01% in short rain, and dry seasons respectively (Table 4.11).

On the other hand, stream flow likely decreases under the SSP5-8.5 scenario during the dry season by 17.2% and 14.05% in the dry season (2040-2070) and (2071-2100), respectively. Both groundwater flow and lateral flow have shown a decreasing pattern over all the future scenarios compared to the baseline period.

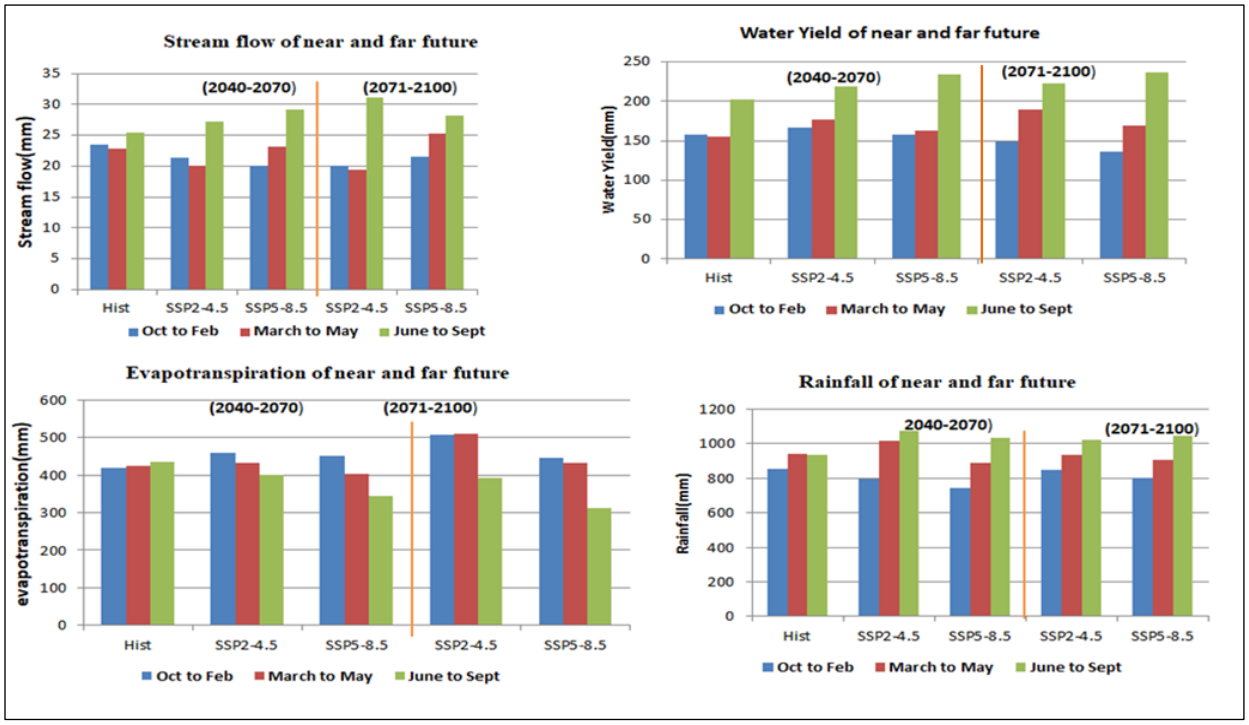

Figure4.9 Projected seasonal impact of climate change on water balance components in Gobele watershed

4.6.3. Impacts Combined Climate and LULC Change on Gobele Water Balance Components

After analyzing the individual effects of climate and LULC change, the combined effect of future climate change (SSP2-4.5 and SSP5-8.5) and future LULC changes (2040 and 2070) in the Gobele watershed was also evaluated. Therefore, using the combined effects of climate change and LULC change, the temporal fluctuation of water balance components was assessed in the three periods (baseline, 2040-2070, and 2071-2100). The results indicated that evapotranspiration would rise in the future under both LULC and climatic scenarios. Furthermore, evapotranspiration will rise in every season under all circumstances. In terms of seasons, the dry season would have a greater variation in evapotranspiration than the short rain and long rain (Table 4.11).

The Gobele watershed's water yield was assessed in relation to the combined effects of LULC and climate change. Water yield in the dry season showed a declining pattern under all scenarios in both the distant future (2071-2100) and midterm future (2040-2070) by the range of 5.24% to 15.41%; in the other scenarios, it exhibits a rising pattern. Seasonally, water yield is expected to grow from 4.64% to 18.28% under short and long rainy seasons in all scenarios and timeframes (Table 4.11).

The Gobele watershed's seasonal stream flow change under future LULC and climate change has been evaluated; under the SSP2-4.5 and SSP5-8.5 scenarios, stream flow is expected to increase from 2.4% to 14.49% by the 2040–2070 time period in short and long rain period respectively (Table4.10). However, at all conditions and times, stream flow tends to decrease by up to 2.4% during the dry season and increases by up to 27.1% during the long rainy season.

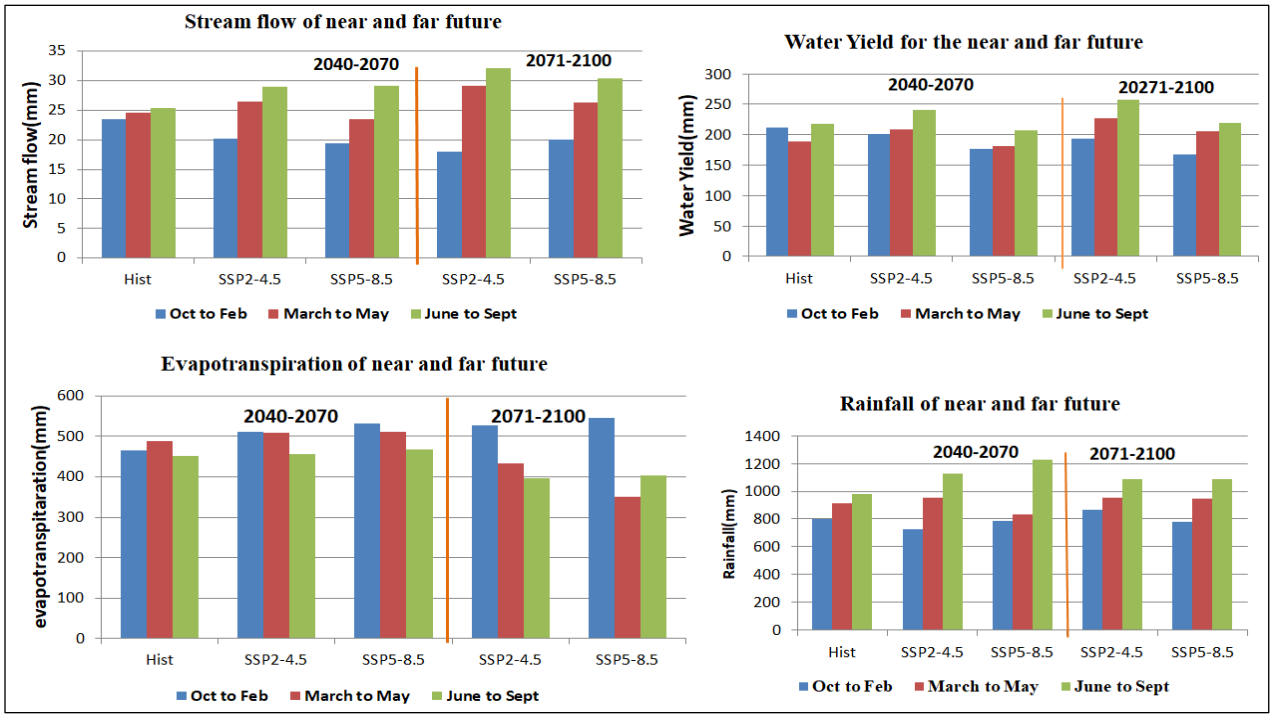

Figure 4.10 Projection of mean seasonal impacts of combined effects of LULC and climate on Gobele water balance components.

Table4.11 The simulated effects of land use land cover **(S1),** climate change **(S2)**, and the combined LULC and climate change **(S3)** on stream flow, evapotranspiration, water yield, and Rainfall of the Gobele watershed.

Scenarios	Months	Periods	Water Balance Components							
			Stream flow		**Evapotranspiration**		**Water yield**		**Precipitation**	
S1	**October to Feb**	1990-2020	24.12		425.84		211.31		942.5	
		2040-2070	18.23		452.5		189.13		836	
		2071-2100	17.71		461.92		188.12		737.9	
	March to May	1990-2020	23.87		376.31		221.23		915.5	
		2040-2070	21.54		398.26		215.78		923.5	
		2071-2100	24.51		409.75		216.39		921	
	June to Sept	1990-2020	28.32		354.19		265.12		984.3	
		2040-2070	34.56		326.45		281.35		1115.5	
		2071-2100	37.12		332.83		301.12		1000.5	
			SSP2-4.5	**SSP5-8.5**	**SSP2-4.5**	**SSP5-8.5**	**SSP2-4.5**	**SSP5-8.5**	**SSP2-4.5**	**SSP5-8.5**
S2	**October to Feb**	1990-2020	23.45	24.45	419.32	411.12	157.43	143.29	852	753.4
		2040-2070	21.31	20.12	459.34	452.34	167.18	158.36	798	745.34
		2071-2100	20.04	21.56	506.21	446.29	148.9	136.83	845	802.5
	Mar to May	1990-2020	22.81	21.08	425.21	399.65	155.02	153.65	943	885.32
		2040-2070	20.11	23.12	431.74	402.92	176.93	163.21	1015	886.3
		2071-2100	19.42	25.32	511.29	432.53	189.12	168.92	934	905.67
	June to Sept	1990-2020	25.45	33.95	434.28	385.03	201.92	217.18	894.6	1008.1
		2040-2070	27.22	29.18	401.25	344.21	218.9	234.11	1076	1032.6
		2071-2100	31.09	28.11	392.4	312.09	223.17	236.87	1023	1043.3
			SSP2-4.5	**SSP5-8.5**	**SSP2-4.5**	**SSP5-8.5**	**SSP2-4.5**	**SSP5-8.5**	**SSP2-4.5**	**SSP5-8.5**
S3	**October to Feb**	1990-2020	23.43	22.67	465.92	485.65	212.24	198.37	723.8	802.84
		2040-2070	20.12	19.39	511.8	526.92	201.11	176.95	802.8	786.28
		2071-2100	17.98	20.02	531.23	544.26	193.57	167.8	868.12	779.32
	March to May	1990-2020	24.56	22.89	489.02	423.94	189.02	177.92	924.82	912.3
		2040-2070	26.52	23.45	508.93	433.23	209.23	181.27	956.7	834.97
		2071-2100	29.11	26.34	512.02	351.2	227.41	206.44	952	945.34
	June to Sept	1990-2020	25.28	28.34	451.81	389.56	217.28	198.03	1022	978.23
		2040-2070	28.944	29.11	456.12	395.92	241.39	207.22	1126	1230
		2071-2100	32.15	30.41	467.12	402.17	256.96	219.67	1089.5	1085.9

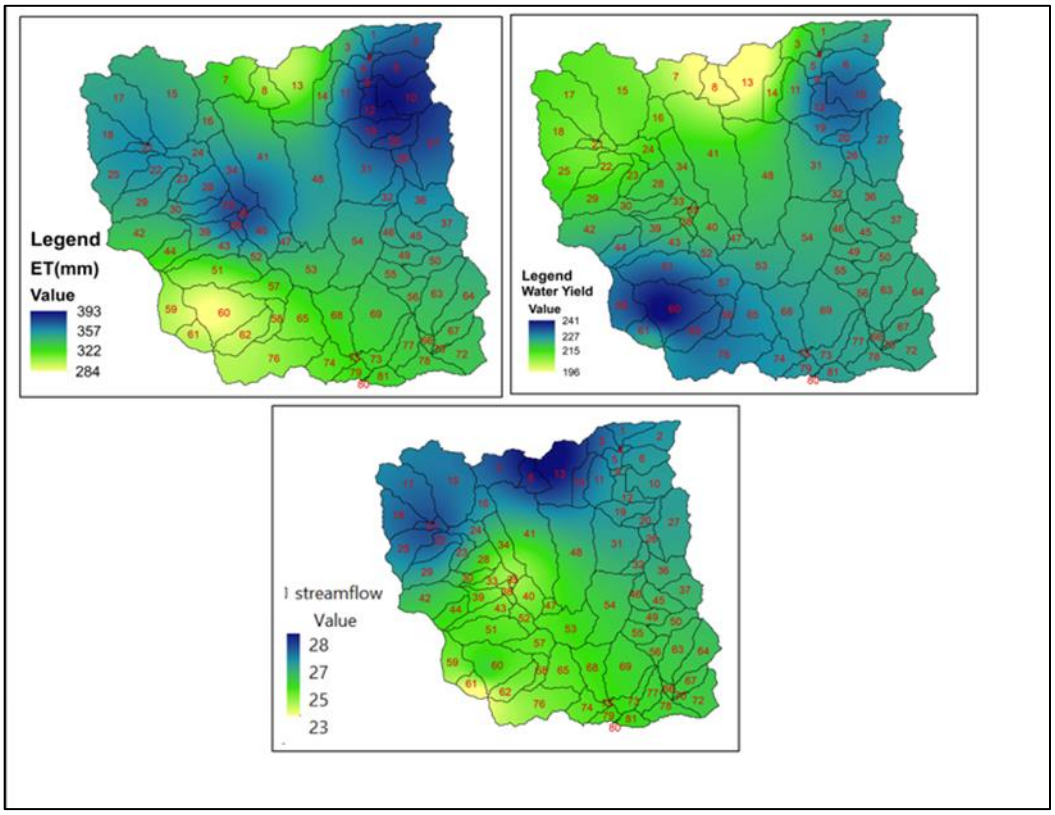

Figure 4.11 Spatial distributions of water balance components

5. CONCLUSION AND RECOMMENDATION

5.1 Conclusion

The study was conducted in the Gobele watershed, Wabe Shebelle River Basin of Ethiopia, to assess the response of water balance components to changes in the individual and combined impacts of climate and land use/land cover pattern. CMIP6 was used to generate high-resolution climate change projections, and the CMhyd tool was used to account for bias. The Cellular Automata-Markov Chain model was used to simulate future land use and land cover for 2040 and 2070. The historical land use land cover was classified from the satellite imagery of 1990, 2005, and 2020 from different sensors. The results revealed that agriculture and settlements will increase, while forest land and grass/shrub land areas will decrease. Using the SWAT model, the combined and isolated effects of LULC and climate change on the water balance components of the Wabe Shebelle River Basin were simulated.

The volume and variability of the monthly observed and simulated stream flow hydrograph time series were effectively captured by the SWAT model in both calibration and validation periods. After evaluating the performance of the GCMs and assessing the accuracy of the classified land use land cover, the multi-model ensemble mean of four GCMs with the land use land cover maps was used to determine future LULC and climate change impacts on water balance components. Historical (1990-2020) trends studies, as well as future (2040–2100) homogeneity tests and trend analyses of annual Rainfall, maximum, and minimum temperatures for the Wabe Gobele watershed under SSP2-4.5 and SSP5-8.5 scenarios, were performed.

The results indicated that the annual average Tmax and Tmin will increase in the future periods, including the precipitation, for all SSP scenarios in the basin, with the exception that the northern-western parts of the basin have shown decreasing patterns. The mean multi-model ensemble of climate models demonstrated good performance in the Gobele watershed.

An excellent agreement was found between the simulated historical data and the observed historical data for the annual mean temperature and Rainfall. An insignificant trend in the annual temperatures (Tmax and Tmin) indicates a significant increase under both SSP 2-4.5 and SSP 5-8.5 scenarios. In contrast, a varying pattern in the mean annual Rainfall

was found at most of the Gobele watershed rainfall stations under SSP5-8.5.

In the three scenarios, the impacts of climate and land use land cover change on the water balance component were analyzed. Results revealed that the mean annual evapotranspiration would increase in the dry season and will decrease in short and long rain seasons in both the midterm future (2040-2070) and distant future (2070–2100) under SSP2-4.5 and SSP5-8.5 climate scenarios. Stream flow and water yield have shown an increasing pattern in long and short rain seasons and a decreasing pattern in dry seasons in all three scenarios in both the far and midterm future under SSP2-4.5 and SSP5-8.5.

The increasing or decreasing patterns of each water balance parameter were different according to the scenarios considered. It was observed that the effects of climate change alone on water balance components demonstrated high effects compared to the land use land cover alone and the combined effects of climate change and land use land cover on water balance components.

5.2 Recommendation

Based on the results obtained in this study, the following recommendations are drown:

- As the strong indicator of climate change is an unpredicted change in temperature and rainfall pattern, the study results show an increment in future temperature and Rainfall. The institution in charge should employ the early warning strategy for the more likely extreme event to occur in the watershed and climate-resilient management techniques like rainwater harvesting for future use, enhance drainage systems, and construct and reinforce existing flood defense infrastructure to lessen the effects of the fast-paced climate change.

- The research findings have revealed that agricultural land and settlements will continuously increase, and forests will decrease. The river basin managers are highly encouraged to employ land use planning regulations, forest conservation and restoration, sustainable agriculture practices, and urban planning and infrastructure development to ensure sustainable water resources management.

- This study evaluated the impacts of climate change on water balance components using CMIP6 climate models, which cannot forecast for the near future. Future researchers are advocated to use of CMIP5, which is capable of forecasting a closer future, compare it with the findings of CMIP6 model datasets, and evaluate their ability to replicate the effects of climate change on climate variables.

- This study offers crucial information about how the water balance components in the Gobele watershed are affected differently by variations in LULC and climate change. However, the LULC classification was done without distinguishing between the different types of crops; the land use and land cover maps assumed that all cultivated cropland and row crops were part of agricultural land. In the future, the hydrologic impact of land use land cover change should be assessed with consideration for a variety of crop varieties and rotations

- This study focused on surface hydrology, which did not include some other water balance components; for the future, it is better to study other hydrological components like groundwater for the better understanding of water resources in the watershed.

6. REFERENCES

Abbaspour, K. C., Rouholahnejad, E., Vaghefi, S., Srinivasan, R., Yang, H., & Kløve, B. (2015).

A continental-scale hydrology and water quality model for Europe: Calibration and uncertainty of a high-resolution large-scale SWAT model. Journal of Hydrology, 524, 733–752.

Access, O., Setegn, S. G., Srinivasan, R., & Dargahi, B. (2008). Hydrological Modelling in theLake Tana Basin, Ethiopia Using SWAT Model. 49–62.

Adams-schoen, S. J., Carlarne, C., & Craig, R. K. (2015). A Response to the IPCC Fifth Assessment. 10027.

Ahmed, K. F., Wang, G., Silander, J., Wilson, A. M., Allen, J. M., Horton, R., & Anyah, R. (2013). Statistical downscaling and bias correction of climate model outputs for climate change impact assessment in the U.S. northeast. Global and Planetary Change, 100, 320–332. https://doi.org/10.1016/j.gloplacha.2012.11.003

Alemayehu, T., Van Griensven, A., Woldegiorgis, B. T., & Bauwens, W. (2017). An improved SWAT vegetation growth module and its evaluation for four tropical ecosystems. Hydrology and Earth System Sciences, 21(9), 4449–4467. https://doi.org/10.5194/hess-21-4449-2017

Arnold, J. G., Moriasi, D. N., Gassman, P. W., Abbaspour, K. C., White, M. J., Srinivasan, R., Santhi, C., Harmel, R. D., Van Griensven, A., Van Liew, M. W., Kannan, N., & Jha, M. K.(2012). SWAT: Model use, calibration, and validation. Transactions of the ASABE, 55(4), 1491–1508.

Belay, T., & Mengistu, D. A. (2021). Impacts of land use/land cover and climate changes on soil erosion in Muga watershed, Upper Blue Nile basin (Abay), Ethiopia. Ecological Processes,10(1). https://doi.org/10.1186/s13717-021-00339-9

Belihu, M., Tekleab, S., Abate, B., & Bewket, W. (2020). Hydrologic response to land use landcover change in the Upper Gidabo Watershed, Rift Valley Lakes Basin, Ethiopia. HydroResearch, 3, 85–94.

Beven, K. (2001). How far can we go in distributed hydrological modelling? Hydrology and Earth System Sciences, 5(1), 1–12. https://doi.org/10.5194/hess-5-1-2001.

Chaemiso, S. E., Abebe, A., & Pingale, S. M. (2016). Assessment of the impact of climate change on surface hydrological processes using SWAT: a case study of Omo-Gibe river basin, Ethiopia. Modeling Earth Systems and Environment, 2(4), 1–15. https://doi.org/10.1007/s40808-016-0257-9

FAO. (2015). Climate change and food security: risks and responses. Rome, Italy: FAO. September, 122. https://www.fao.org/3/i5188e/i5188e.pdf

Fentaw, F., Hailu, D., Nigussie, A., & Melesse, A. M. (2018). Climate Change Impact on the Hydrology of Tekeze Basin, Ethiopia: Projection of Rainfall-Runoff for Future Water Resources Planning. Water Conservation Science and Engineering, 3(4), 267–278. https://doi.org/10.1007/s41101-018-0057-3

Fita, T., & Abate, B. (2022a). Impact of climate change on streamflow of Melka Wakena catchment, Upper Wabi Shebelle sub-basin, south-eastern Ethiopia. Journal of Water and Climate Change, 13(5), 1995–2010. https://doi.org/10.2166/wcc.2022.191

Fita, T., & Abate, B. (2022b). Impact of climate change on streamflow of Melka Wakena catchment, Upper Wabi Shebelle sub-basin, south-eastern Ethiopia. Journal of Water and Climate Change, 13(5), 1995–2010.

Germer, S., Neill, C., Krusche, A. V, & Elsenbeer, H. (2010). Influence of land-use change on midterm-surface hydrological processes: undisturbed forest to pasture. Journal of Hydrology,380(3–4), 473–480.

Getachew, B., Manjunatha, B. R., & Bhat, H. G. (2021). Modeling projected impacts of climate and land use/land cover changes on hydrological responses in the Lake Tana Basin, upper Blue Nile River Basin, Ethiopia. Journal of Hydrology, 595, 125974.

Getahun, Y. S., & HAJ, V. L. (2015). Assessing the Impacts of Land Use-Cover Change on Hydrology of Melka Kuntrie Subbasin in Ethiopia, Using a Conceptual Hydrological Model. Journal of Waste Water Treatment & Analysis, 06(03). https://doi.org/10.4172/2157-7587.1000210

Ghosh, S., & Mujumdar, P. P. (2009). Climate change impact assessment: Uncertainty modeling with imprecise probability. Journal of Geophysical Research Atmospheres, 114(18), 1–17. https://doi.org/10.1029/2008JD011648

Gizaw, M. S., Biftu, G. F., Gan, T. Y., Moges, S. A., & Koivusalo, H. (2017). Potential impact of climate change on streamflow of major Ethiopian rivers. Climatic Change, 143, 371–383.

Guduru, J. U., & Jilo, N. B. (2022). Groundwater potential zone assessment using integrated analytical hierarchy process-geospatial driven in a GIS environment in Gobele watershed, Wabe Shebele river basin, Ethiopia. Journal of Hydrology: Regional Studies, 44(September), 101218. https://doi.org/10.1016/j.ejrh.2022.101218

Gurara, M. A., Jilo, N. B., & Tolche, A. D. (2021). Impact of climate change on potential evapotranspiration and crop water requirement in Upper Wabe Bridge watershed, Wabe

Shebele River Basin, Ethiopia. Journal of African Earth Sciences, 180(October 2020), 104223. https://doi.org/10.1016/j.jafrearsci.2021.104223

Halefom, A., & Teshome. (2018). Applications of Remote Sensing and GIS in Land Use / Land Cover Change Detection. Applied Research Journal of Geographic Information System, 1(1), 1–9.

Hayicho, H., Alemu, M., & Kedir, H. (2019). Assessing the Effects of Land-Use and Land CoverChange and Topography on Soil Fertility in Melka Wakena Catchment of Sub-Upper Wabe-Shebelle Watershed, South Eastern Ethiopia. Journal of Environmental Protection, 10(05), 672–693. https://doi.org/10.4236/jep.2019.105040

Healy, R. W., & Essaid, H. I. (2012). VS2DI: Model use, calibration, and validation.Transactions of the ASABE, 55(4), 1249–1260. https://doi.org/10.13031/2013.42256

Hordofa, A. T., Leta, O. T., Alamirew, T., & Chukalla, A. D. (2022). Spatiotemporal Trend Analysis of Temperature and Rainfall over Ziway Lake Basin, Ethiopia. Hydrology, 9(1). https://doi.org/10.3390/hydrology9010002

Huyen, N. T., Tu, L. H., Tram, V. N. Q., Minh, D. N., Liem, N. D., & Loi, N. K. (2017).

Assessing the impacts of climate change on water resources in the Srepok watershed,Central Highland of Vietnam. Journal of Water and Climate Change, 8(3), 524–534.

IPCC. (2014). Part A: Global and Sectoral Aspects. (Contribution of Working Group II to the Fifth Assessment Report of the Intergovernmental Panel on Climate Change). Climate Change 2014: Impacts, Adaptation, and Vulnerability., 1132. https://www.ipcc.ch/pdf/assessment-report/ar5/wg2/WGIIAR5-FrontMatterA_FINAL.pdf

IPCC, T. A. R. (2007). Climate change 2007: synthesis report. In Contribution of working groups I, II and III to the fourth assessment report of the intergovernmental panel onclimate change (p. 104). ipcc Geneva, Switzerland.

Jenness, J., & Wynne, J. J. (2007). Kappa analysis (kappa_stats. avx) extension for ArcView 3.

x. Jenness Enterprises.
Kenea, U., Adeba, D., Regasa, M. S., & Nones, M. (2021). Hydrological responses to land use land cover changes in the fincha'a watershed, Ethiopia. Land, 10(9), 60–81. https://doi.org/10.3390/land10090916

Kim, U., & Kaluarachchi, J. J. (2009). Climate change impacts on water resources in the upper blue Nile River Basin, Ethiopia 1. JAWRA Journal of the American Water Resources Association, 45(6), 1361–1378.

Kiros, G., Shetty, A., & Nandagiri, L. (2015). Performance Evaluation of SWAT Model for LandUse and Land Cover Changes under different Climatic Conditions: A Review. Journal of Waste Water Treatment & Analysis, 06(03). https://doi.org/10.4172/2157-7587.1000216

Kuma, H. G., Feyessa, F. F., & Demissie, T. A. (2023). Assessing the impacts of land use/land cover changes on hydrological processes in Southern Ethiopia: The SWAT model approach.Cogent Engineering, 10(1). https://doi.org/10.1080/23311916.2023.2199508

Kusuma, S., Sundara Kumar, K., Udaya Bhaskar, P., & Padmakumari, K. (2016).

APPLICATION OF LAND CHANGE MODELER FOR PREDICTION OF FUTURE LAND

USE LAND COVER A CASE STUDY OF VIJAYAWADA CITY Modeling of Urban Climate of new capital city of Andhra Pradesh View project APPLICATION OF LAND CHANGE MODELER FOR PREDICTION OF FUTURE LAND U. February, 2571–2581. https://www.researchgate.net/publication/293821367

Kyu, H. H., Pinho, C., Wagner, J. A., Brown, J. C., Bertozzi-Villa, A., Charlson, F. J., Coffeng,

L. E., Dandona, L., Erskine, H. E., & Ferrari, A. J. (2016). Global and national burden of diseases and injuries among children and adolescents between 1990 and 2013: findings from the global burden of disease 2013 study. JAMA Pediatrics, 170(3), 267–287.

Lee, J., Lintner, B. R., Boyce, C. K., & Lawrence, P. J. (2011). Land use change exacerbates tropical South American drought by sea surface temperature variability. Geophysical Research Letters, 38(19).

Legg, S. (2021). IPCC, 2021: Climate change 2021-the physical science basis. Interaction, 49(4),44–45.

Leta, M. K., Demissie, T. A., & Tränckner, J. (2021). Modeling and prediction of land use landcover change dynamics based on land change modeler (Lcm) in nashe watershed, upper blue nile basin, Ethiopia. Sustainability (Switzerland), 13(7). https://doi.org/10.3390/su13073740

Lin, W., Zhang, L., Du, D., Yang, L., Lin, H., Zhang, Y., & Li, J. (2009). Quantification of land use/land cover changes in Pearl River Delta and its impact on regional climate in summer using numerical modeling. Regional Environmental Change, 9, 75–82.

Liping, C., Yujun, S., & Saeed, S. (2018). Monitoring and predicting land use and land cover changes using remote sensing and GIS techniques—A case study of a hilly area, Jiangle, China. PLoS ONE, 13(7), 1–23. https://doi.org/10.1371/journal.pone.0200493

Manakos, I., & Braun, M. (2014). Land use and land cover mapping in Europe (Vol. 18).

Springer.
Maraun, D., Shepherd, T. G., Widmann, M., Zappa, G., Walton, D., Gutiérrez, J. M., Hagemann, S., Richter, I., Soares, P. M. M., & Hall, A. (2017). Towards process-informed bias correction of climate change simulations. Nature Climate Change, 7(11), 764–773.

Miller, K., Miller, K. A., & Yates, D. (2014). Climate Change and Water Resources : A Primerfor Water Utilities CLIMATE CHANGE AND WATER RESOURCES : A Primer for Water Utilities Preliminary Draft Not for citation or reproduction – all figure permissionsare pending National Center for Atmospheric Res. The National Center for Atmospheric Research, January 2005.

Mishra, V. N., & Rai, P. K. (2016). A remote sensing aided multi-layer perceptron-Markov chainanalysis for land use and land cover change prediction in Patna district (Bihar), India. Arabian Journal of Geosciences, 9, 1–18.

Mitiku, A. B., Meresa, G. A., Mulu, T., & Woldemichael, A. T. (2023). Examining the impacts of climate variabilities and land use change on hydrological responses of Awash River basin, Ethiopia. HydroResearch, 6, 16–28. https://doi.org/10.1016/j.hydres.2022.12.002

Moriasi, D. N., Arnold, J. G., Van Liew, M. W., Bingner, R. L., Harmel, R. D., & Veith, T. L. (2007). Model evaluation guidelines for systematic quantification of accuracy in watershedsimulations. Transactions of the ASABE, 50(3), 885–900.

Moss, R. H., Edmonds, J. A., Hibbard, K. A., Manning, M. R., Rose, S. K., Van Vuuren, D. P., Carter, T. R., Emori, S., Kainuma, M., & Kram, T. (2010). The next generation of scenarios for climate change research and assessment. Nature, 463(7282), 747–756.

NAPA. (2007). Climate change National Adapation Programme of Action of Ethiopia. GlobalEnvironmental Facility(GEF), 2(June), 96.

Nguyen, T. (2015). Optimal ground control points for geometric correction using genetic algorithm with global accuracy. European Journal of Remote Sensing, 48(1), 101–120.

O'Neill, B. C., Carter, T. R., Ebi, K., Harrison, P. A., Kemp-Benedict, E., Kok, K., Kriegler, E.,Preston, B. L., Riahi, K., Sillmann, J., van Ruijven, B. J., van Vuuren, D., Carlisle, D., Conde, C., Fuglestvedt, J., Green, C., Hasegawa, T., Leininger, J., Monteith, S., & Pichs-Madruga, R. (2020). Achievements and needs for the climate change scenario framework. Nature Climate Change, 10(12), 1074–1084. https://doi.org/10.1038/s41558-020-00952-0

Orkodjo, T. P., Kranjac-Berisavijevic, G., & Abagale, F. K. (2022). Impact of climate change onfuture precipitation amounts, seasonal distribution, and streamflow in the Omo-Gibe basin, Ethiopia. Heliyon, 8(6), e09711. https://doi.org/10.1016/j.heliyon.2022.e09711

Pal, J. S., Giorgi, F., Bi, X., Elguindi, N., Solmon, F., Gao, X., & Rauscher. S.A. (2007). Climate for the Developing. Bulletin of the American Meteorological Society, 88(9), 1395–1409.

Paul, M., Rajib, M. A., & Ahiablame, L. (2017). Spatial and temporal evaluation of hydrological response to climate and land use change in three South Dakota watersheds. JAWRA Journalof the American Water Resources Association, 53(1), 69–88.

Pierce, D. W., Barnett, T. P., Santer, B. D., & Gleckler, P. J. (2009). Selecting global climate models for regional climate change studies. Proceedings of the National Academy of Sciences of the United States of America, 106(21), 8441–8446. https://doi.org/10.1073/pnas.0900094106

Pörtner, H.-O., Scholes, R. J., Agard, J., Archer, E., Arneth, A., Bai, X., Barnes, D., Burrows, M., Chan, L., & Cheung, W. L. (2021). IPBES-IPCC co-sponsored workshop report on biodiversity and climate change. IPBES and IPCC, 10.

Rathjens, H., Bieger, K., Srinivasan, R., & Arnold, J. G. (2016). CMhyd User Manual: Documentation for preparing simulated climate change data for hydrologic impact studies.p.16p.

Reshmidevi, T. V., Nagesh Kumar, D., Mehrotra, R., & Sharma, A. (2018). Estimation of the climate change impact on a catchment water balance using an ensemble of GCMs. Journal of Hydrology, 556, 1192–1204. https://doi.org/10.1016/j.jhydrol.2017.02.016

Rhymee, H., Shams, S., Ratnayake, U., & Rahman, E. K. A. (2022). Comparing Statistical Downscaling and Arithmetic Mean in Simulating CMIP6 Multi-Model Ensemble over Brunei. Hydrology, 9(9). https://doi.org/10.3390/hydrology9090161

Ritchie, H., Roser, M., & Rosado, P. (2020). CO_2 and greenhouse gas emissions. Our World inData.

Romañach, S. S., McKelvy, M., Suir, K., & Conzelmann, C. (2015). EverVIEW: A visualization platform for hydrologic and Earth science gridded data. Computers & Geosciences, 76, 88–95.

Samal, D. R., & Gedam, S. S. (2015). Monitoring land use changes associated with urbanization: An object based image analysis approach. European Journal of Remote Sensing, 48(1), 85–99.

Schoof, J. T. (2013). Statistical downscaling in climatology. Geography Compass, 7(4), 249–

265. https://doi.org/10.1111/gec3.12036

Shiferaw, H., Gebremedhin, A., Gebretsadkan, T., & Zenebe, A. (2018). Modelling hydrologicalresponse under climate change scenarios using SWAT model: the case of Ilala watershed, Northern Ethiopia. Modeling Earth Systems and Environment, 4, 437–449.

Shigute, M., Alamirew, T., Abebe, A., Ndehedehe, C. E., & Kassahun, H. T. (2022).

Understanding Hydrological Processes under Land Use Land Cover Change in the Upper Genale River Basin, Ethiopia. Water (Switzerland), 14(23), 1–27. https://doi.org/10.3390/w14233881

Singh, A. K., Dagar, J. C., Arunachalam, A., Gopichandran, R., & Shelat, K. N. (2015). Climatechange modelling, planning and policy for agriculture. Climate Change Modelling, Planning and Policy for Agriculture, 1–625. https://doi.org/10.1007/978-81-322-2157-9

Sisay, E., Halefom, A., Khare, D., Singh, L., & Worku, T. (2017). Hydrological modelling of ungauged urban watershed using SWAT model. Modeling Earth Systems and Environment,3(2), 693–702. https://doi.org/10.1007/s40808-017-0328-6

Taylor, K. E., Stouffer, R. J., & Meehl, G. A. (2012). An overview of CMIP5 and the experimentdesign. Bulletin of the American Meteorological Society, 93(4), 485–498.

Temesgen, M., Hoogmoed, W. B., Rockstrom, J., & Savenije, H. H. G. (2009). Conservation tillage implements and systems for smallholder farmers in semi-arid Ethiopia. Soil and Tillage Research, 104(1), 185–191.

Tesfaw, B. A., Dzwairo, B., & Sahlu, D. (2023). Assessments of the impacts of land use/land cover change on water resources: Tana Sub-Basin, Ethiopia. Journal of Water and Climate Change, 14(2), 421–441. https://doi.org/10.2166/wcc.2023.303

Thanapakpawin, P., Richey, J., Thomas, D., Rodda, S., Campbell, B., & Logsdon, M. (2007). Effects of landuse change on the hydrologic regime of the Mae Chaem river basin, NW Thailand. Journal of Hydrology, 334(1–2), 215–230.

Thuiller, W. (2007). Climate change and the ecologist. Nature, 448(7153), 550–552.

Tola, S. Y., & Shetty, A. (2021). Land cover change and its implication to hydrological regimesand soil erosion in Awash River basin, Ethiopia: a systematic review. Environmental Monitoring and Assessment, 193(12). https://doi.org/10.1007/s10661-021-09599-6

Tolosa, A. T. (2018). Evaluating the Dynamics of Land Use/Land Cover Change Using GIS andRemote Sensing Data in Case of Yewoll Watershed, Blue Nile Basin, Ethiopia.

Toni, A. T., Malcherek, A., & Kassa, A. K. (2022). Agroclimatic Zone-Based Analysis of Rainfall Variability and Trends in the Wabi Shebele River Basin, Ethiopia. Water

(Switzerland), 14(22), 1–16. https://doi.org/10.3390/w14223699

Trenberth, K. E. (2011). Changes in precipitation with climate change. Climate Research, 47(1–2), 123–138. https://doi.org/10.3354/cr00953

Trisos, C. H., Adelekan, I. O., Totin, E., Ayanlade, A., Efitre, J., Gemeda, A., Kalaba, K.,Lennard, C., Masao, C., Mgaya, Y., Ngaruiya, G., Olago, D., Simpson, N. P., & Zakieldeen,

S. (2022). Nine principles for encouraging a context-driven, inclusive and proactive approach to planning for climate risk in African cities. In Climate Change 2022: Impacts, Adaptation and Vulnerability. https://doi.org/10.1017/9781009325844.011.1286

Trzaska, S., & Schnarr, E. (2014). A review of downscaling methods for climate change projections. United States Agency for International Development by Tetra Tech ARD, September, 1–42.

Wainwright, C. M., Black, E., & Allan, R. P. (2021). Future changes in wet and dry season characteristics in CMIP5 and CMIP6 simulations. Journal of Hydrometeorology, 22(9),2339–2357.

Walton, D. B., Sun, F., Hall, A., & Capps, S. (2015). A hybrid dynamical-statistical downscaling technique. Part I: Development and validation of the technique. Journal of Climate, 28(12),4597–4617. https://doi.org/10.1175/JCLI-D-14-00196.1

Welde, K., & Gebremariam, B. (2017). Effect of land use land cover dynamics on hydrologicalresponse of watershed: Case study of Tekeze Dam watershed, northern Ethiopia. International Soil and Water Conservation Research, 5(1), 1–16.

White, K. L., & Chaubey, I. (2005). Sensitivity analysis, calibration, and validations for a multisite and multivariable SWAT model. Journal of the American Water Resources Association, 41(5), 1077–1089. https://doi.org/10.1111/j.1752-1688.2005.tb03786.x

Woldemariam, G. W., & Harka, A. E. (2020). Effect of land use and land cover change on soil erosion in erer sub-basin, Northeast Wabi Shebelle Basin, Ethiopia. Land, 9(4). https://doi.org/10.3390/land9040111

Woldemariam, G. W., Iguala, A. D., Tekalign, S., & Reddy, R. U. (2018). Spatial modeling of soil erosion risk and its implication for conservation planning: The case of the gobele watershed, east hararghe zone, ethiopia. Land, 7(1). https://doi.org/10.3390/LAND7010025

Woodfine, A. (2009). Using sustainable land management practices to adapt to and mitigate climate change in sub-Saharan Africa: Resource Guide Version 1.0. TerrAfrica, Washington DC, USA.

Yohannes, A. W., Cotter, M., Kelboro, G., & Dessalegn, W. (2018). Land use and land cover changes and their effects on the landscape of Abaya-Chamo basin, Southern Ethiopia. Land,7(1). https://doi.org/10.3390/land7010002

Zhang, Y., You, Q., Chen, C., & Ge, J. (2016). Impacts of climate change on streamflows underRCP scenarios: A case study in Xin River Basin, China. Atmospheric Research, 178, 521–534.

7. APPENDICES

Appendix1: SWAT model parameters with their initial values

no	Parameters	Descriptions	Initial range
1	R__CN2.mgt	SCS runoff curve number	-2.2
2	V__ALPHA_BF.gw	Baseflow alpha factor (days)	0–1
3	V__GW_DELAY.gw	Groundwater delay (days)	0–500
4	V__GWQMN.gw	Threshold depth of water in the shallow aquifer	0–5000
		required for return flow to occur (mm)	
5	R__GW_REVAP.gw	Groundwater “revap” coefficient	0.2–0.4
6	R__RCHRG_DP.gw	Deep aquifer percolation fraction	0-1
7	R__CH_K2.rte	Effective hydraulic conductivity in main channel alluvium	0.01–500
8	R__ALPHA_BNK.rte	Baseflow alpha factor for bank storage (days)	0–1
9	R__SOL_AWC(..).sol	Available water capacity of the soil layer	-0.2–2
10	SLSUBBSN.hru	Average slope length	10–150
11	V__ESCO.hru	Soil evaporation compensation factor	0–1
12	R__REVAPMN.gw	Threshold water in the shallow aquifer for revap to occur (mm)	0–500
13	R__CH_W1.sub	Average width of tributary channels (m)	-0.08
14	V__CH_N1.sub	Main channel .Manning’s coefficient	0-1
15	R__SURLAG.bsn	Surface runoff lag time	0.05–24
16	R__HRU_SLP.hru	Average slope steepness	0–1
17	R__OV_N.hru	Manning's "n" value for overland flow	0.01–100
18	A__EPCO.bsn	Plant compensation factor at main channel	0–1
19	V__CANMX.hru	Maximum canopy storage	0–100
20	R__SOL_BD.sol	Moist bulk density	-0.5–0.6

Where V_Replace: replaces the parameter's current value with a specified value, and R_Relative: updates the parameter's value by multiplying the fixed values (in each HRU) by the same coefficient, and A_Absolute: adds the given value to existing value.

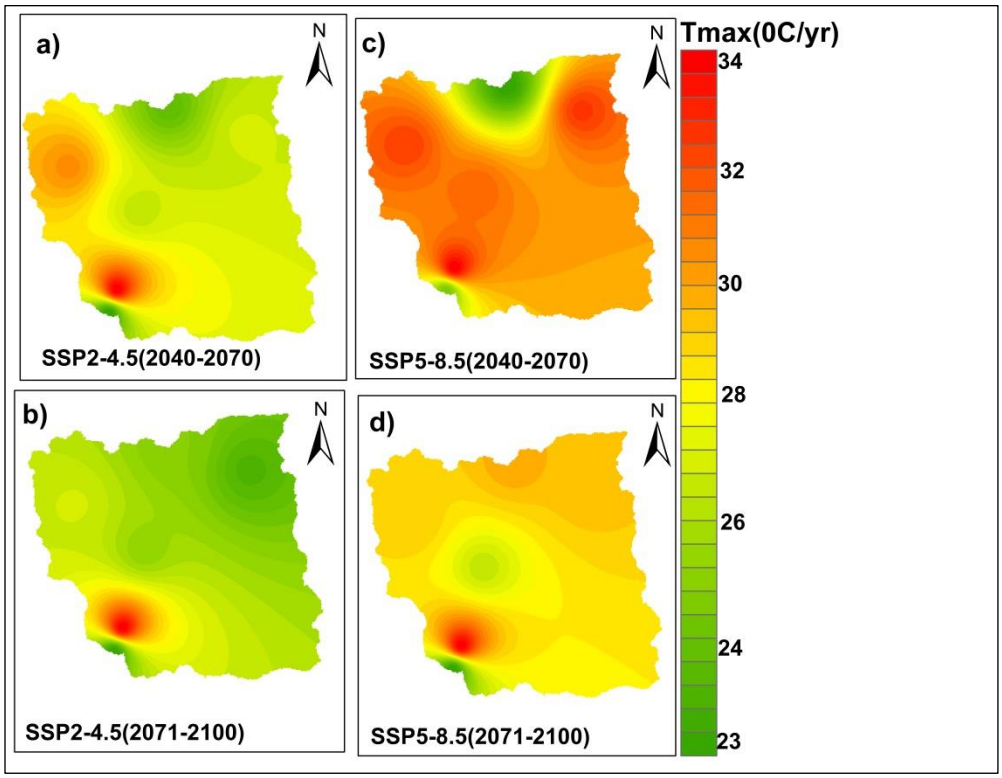

Appendix 1 The Spatial distribution of the multi-model ensemble means annual Tmax **a)** midterm future SSP2-4.5, **b)** distant future SSP2-4.5, **c)** midterm future SSP5-8.5 and **d)** distant future SSP5-8.5

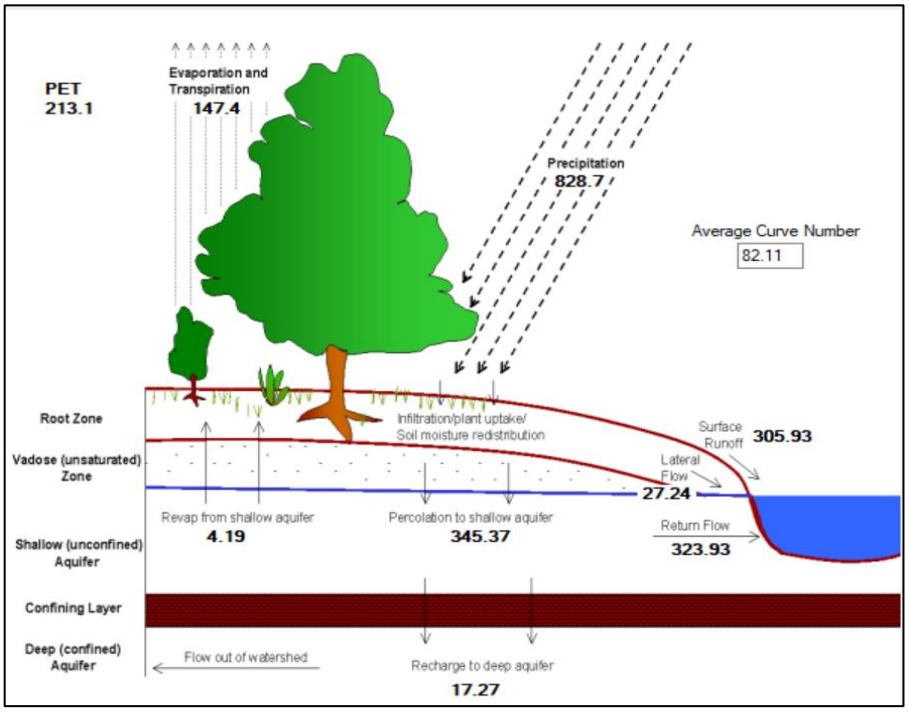

Appendix 2 The SWAT model hydrology of the Gobele watershed

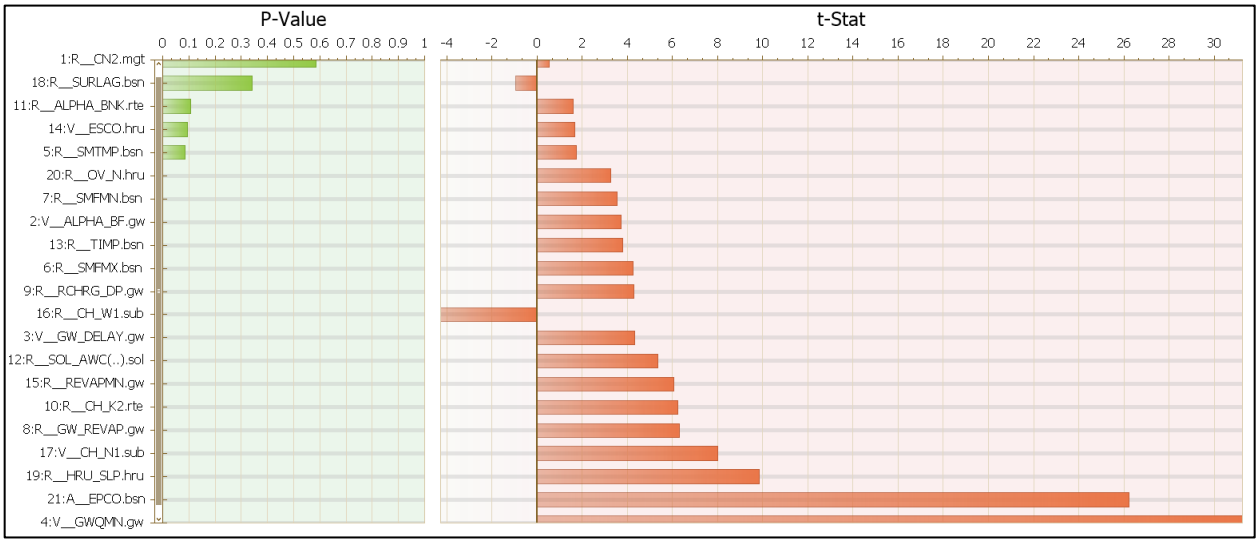

Figure Appendix 3 SWAT sensitivity parameters from the SWAT-CUP